UNIVERSITÀ DEGLI STUDI
DI MILANO

DOTTORATO DI RICERCA IN INFORMATICA
XIX CICLO
SETTORE SCIENTIFICO DISCIPLINARE INF/01 INFORMATICA

Color in context and spatial color computation

Tesi di Dottorato di Ricerca di:
Davide Gadia

Relatore:
Prof. Daniele Marini

Correlatore:
Prof. Alessandro Rizzi

Coordinatore del Dottorato:
Prof. Vincenzo Piuri

Anno Accademico 2005/06

Contents

Chapter 1

Introduction

Correct color representation is one of the most interesting and discussed problems in the imaging and computer graphics field. It has been extensively proven that there is a clear distinction between what is called the *color stimulus*, i.e. the response of the cones in the retina, and what is the *perceived color*, i.e. the result of the complex mechanisms of analysis and perception of the Human Visual System.

This perception is mainly driven by the context in which a "color" is observed. Many theories and models have been proposed in the years for the analysis and computation of effective perceived colors in context: Retinex is one of the most relevant.

These models have been implemented into algorithms and applied in many ways in digital imaging and computer graphics field.

However, a relevant limitation of most of the computational methods proposed is the restriction of working on the low luminance dynamic range allowed by common RGB images. These values are not comparable to the large dynamic range of real scenes to which our visual system adapts. To better simulate perception mechanisms and to implement accurate computational models of color perception, there is the need to work with the so-called *High Dynamic Range* (HDR) images, in which each pixel stores a floating point value equivalent to the real luminance of the acquired or simulated scene.

These kinds of images can be generated using advanced global illumination algorithms, or can represent real scenes, and normally they are acquired by using well-known reconstruction methods from multiple exposures shots. However some advanced but still expensive sensors are already available and able to acquire the entire high dynamic range of a scene in a single pass, without the application of interpolations or reconstructions, that lead to inevitable numerical errors. It is not a hazard to predict that in a not-so-far future this kind of technology will be more affordable and diffuse in the large market field. Obviously, the need for a correct and accurate computational model for a correct color reproduction will be crucial.

A great effort has been done in the last fifteen years in the development of computational models that try to simulate many perceptual mechanisms in the conversion of

the unsupported floating point values of HDR data into the accepted dynamic range of the available output devices (monitors, printers, etc.). These algorithms are known as *tone mapping* operators. However, most of the proposed operators address luminance mapping only, without considering the crucial relevance of a correct color computation.

The purpose of this dissertation is to contribute in the field of spatial color computation models.

We will begin introducing some background about color in context research and experiments, and we will give an overview about different approaches in the definition of computational models of color in digital imaging.

In particular, we will present a recent accurate mathematical definition and analysis of the Retinex algorithm, that leads to the definition of a new computational model called *Random Spray Retinex (RSR)*.

We will then introduce the tone mapping problem, discussing the lack and the need for color computation in the implementation of a correct computational model that tries to simulate perceptual response: at this aim, we will present a Retinex implementation called *HDR Retinex*. The algorithm is based on the well-known Brownian Retinex computational model, modified taking inspiration from the eye movements and scene sampling, in order to tune the intrinsic color correction behavior of Retinex algorithms for a correct mapping of HDR values into accepted dynamic range.

A recent research has demonstrated a relevant variability in the spatial distribution of cones in human retina among different subjects, with consequent subjective differences in retinal color stimuli during observation. This could suggest a corresponding difference in color perception, but however a similar phenomenon has not been observed: therefore it has been suggested that perceptual mechanisms exists that compensate these variations in the receptors stimuli. To investigate this hypothesis, we present some experiments analyzing the influence of spatial color computation on *tristimulus values* obtained using different integrating curves (the so-called *Color Matching Functions (CMFs)*) on spectral luminance distribution generated by a photometric raytracer.

The results of these experiments show a significant decrease of the interdifference

when a contextual color correction is applied, based on Von Kries or HDR Retinex methods, and therefore they prove the extreme relevance of considering and applying a correct color computational model in the imaging and computer graphics fields.

Chapter 2

Color in context

Contents

Color research has a long and mostly debated history. Many important contributions in this field have been proposed by some of the most relevant scientists in the history. Almost all of them tried to come to terms with the *paradox* (as it was defined by Semir Zeki[136]) of color vision. From 1700 it was a common assumption that the color of an object was generated by the dominant wavelength of the reflected light incoming the eye, and many theories have been proposed guessing if, how and how many receptors were included in the human eye. However, the paradox is introduced by the fact that observing objects under different conditions of illumination, we perceive the same color even if the wavelength composition of the incoming light presents relevant variations. This phenomenon, known as *color constancy*, is actually considered one of the more important properties of our visual system.

Many scientists noticed this phenomenon and tried to explain it, realizing that something *more* than just the physical nature of light was involved, but unfortunately, due to the lack of knowledge and scientific instruments of their times, a correct explanation had to wait several decades.

In this chapter we don't present a full overview of color research history (for every argument presented in the next sections, several books have been written, and probably many others will be), but we just summarize the works and contributions of the main scientists involved in this field, considering if and how they tried to explain color constancy effects.

We will also present a description of some psychophysical experiments directly correlated to the analysis of how subjective color perception and classical explanations of color vision do not collide, and that are at the basis of the most relevant theories regarding the perception mechanisms of the Human Visual System (HVS).

These theories have been used to develop color in context computational models for image processing and computer graphics softwares; in the last section of this chapter we will present a brief description of the main approaches.

2.1 Historical overview of color research

In this section we summarize the main scientific steps in color research field, without deep investigations, but rather focusing our attention on the eventual consideration of color constancy effects. We can roughly consider two different approaches in the definition of color theories in history: the *physical* approach, characterized by a direct correlation between color and spectral characterization of light incoming human eyes, and the *psychological* approach, based on the contrary on the analysis of color interactions.

2.1.1 Physical approach

Isaac Newton

With Newton's prism experiments in 1672[81] we can indentify the beginning of the color research history.

Newton's approach is strictly based on a physical phenomenon, i.e. the observation of the *spectrum* of consecutive colors obtained after the refraction of light passing through a prism. His conclusions, after some experiments, was that white light is composed of single, "pure", coloured lights, that can be mixed to form secondary colors.

However, the final proposal of his famous *circular arrangement of spectral colours* (see fig. 2.1), with seven basilar colors on the border and white in the center, has also a strong aesthetic component: Newton's belief was that the propagation of both light and sound were comparable, and therefore he chose the number of basilar colors and their disposition in the circle in accordance to Dorian musical scale.

Even if Newton's assumption was that light was composed by tiny corpuscles, his theory of a strict relation between color and physical nature of light became the basic background of most of the color researches proposed in the following decades.

With the introduction of experiments and theories regarding the wave nature of light, it was clear that the spectral colors on the border of Newton's circle simply represent specific wavelengths in the reflected light, and therefore it was assumed that color of an

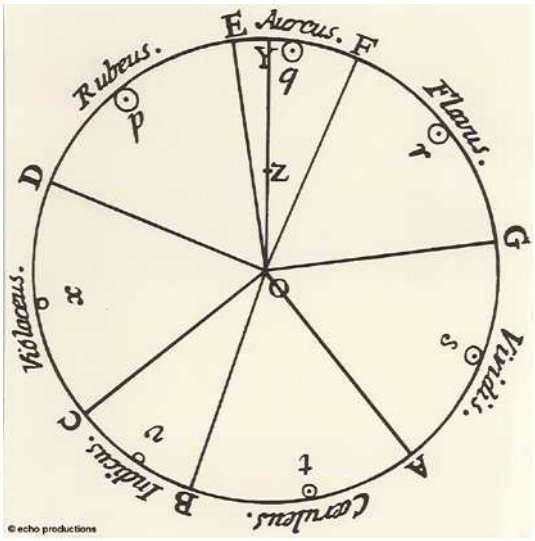

Figure 2.1: *Newton's color circle.*

object was directly dipendent on the dominant wavelength of the incoming light energy.

Thomas Young

For a century, Newton's theory had not been discussed. In 1802 Thomas Young[133] criticed Newton's theory that human eye has receptors for each possible spectral color, and suggested that only a limited number of elements in the eye are responsible for color vision.

His hypothesis was that all colors sensations can be generated combining three spectral colors, and that therefore only three receptors oscillating with the respective wave are present in human eye. He identified this three spectral colors in red, yellow and blue at first, then he changed to red, green and violet.

It was the first time that an hypothesis regarding inner eye physiology had been proposed in the definition of a color theory, and it is very remarkable considering that a concrete confirmation of the presence of cones in the retina is dated 1960.

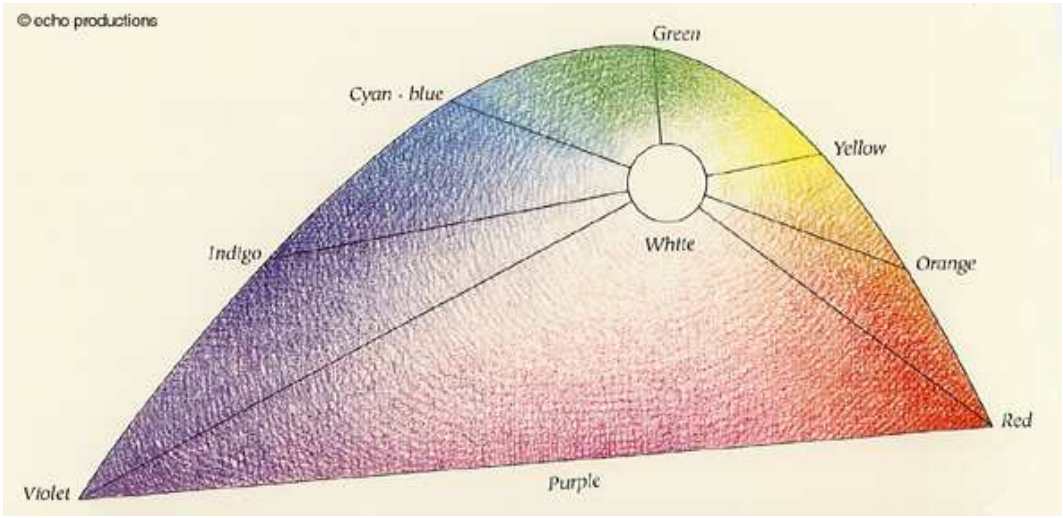

Figure 2.2: *Helmholtz's color triangle.*

Hermann von Helmholtz

Even if in 1852 he rejected[124] Young's trichromatic color definition, trying to redefine Newton's circle with five spectral colors instead of the original seven, in 1866 Hermann von Helmholtz, after deeper evaluations, decided to adopt Young's theory of the presence of three receptors in the human eye, responsible of color vision. His contribution[124] was so relevant that actually the trichromatic theory is known as *Young-Helmholtz* theory (see fig. 2.2).

Helmholtz was one of the first to notice and suggest that a clear distinction between physical phenomenon (i.e. spectral composition of light) and subjective effects must be considered regarding color perception. His assumption was that color sensation was caused by peculiar reactions of visual nerves due to different spectral stimuli.

In particular, he was very interested by color constancy phenomenon, and tried to solve it. However, his hypothesis was quite vague and not clear: he suggested that color constancy was caused by a sort of "discounting of the illuminant" factor, due to a process called *unconscious inference*[124,136].

James Clerck Maxwell

The contribution in color research by James Clerck Maxwell in 1860 is crucial: with his experiments he put the basis for modern colorimetry[72].

His research gave an experimental demonstration that Newton's circle of seven colors, with white as a middle point, implicitly satisfied the trichromatic theory proposed by Young, concluding in some sense the long discussions between scientists supporting Newton's theory and those who instead agreed with Young's proposal.

Moreover, in his further experiments into the measurement of color, Maxwell proposed an experimental setup that actually is still the basis for the definition of Color Matching Functions in colorimetry field, based on the match between a target and the mixture of three basilar spectral stimuli[72,131]. In chapter 5 we will discuss about colorimetry research and contextual color computation.

2.1.2 Psychological approach

Johann Wolfgang von Goethe

It is not easy to summarize in few paragraphs the *Theory of Colors* proposed by Goethe in 1810[43]. His contribution, that was not well accepted by the physics community of his time and rarely considered in modern discussion regarding color science, is closer to the real understanding of color sensation than most of the previously cited scientists.

His experiments regarding prisms refractions, after-images, colored shadows and complementary colors were in the direction of a more conclusive and complete consideration of color as the union of physical phenomenons (i.e. the characteristics of incoming light), physiological mechanisms (i.e. the response of human eye to the light stimuli) and psycological behaviors (i.e. perception mechanisms of the visual system).

In the definition of his color circle (see fig. 2.3), Goethe tried to establish a set of laws of *color harmony*, so that positions of colors are directly correlated to a subjective psychological interpretation (e.g. yellow associated with *"light"* or *"warmth"* and blue with *"shadow"* or *"cold"*), based on the underlying assumption that color is generated

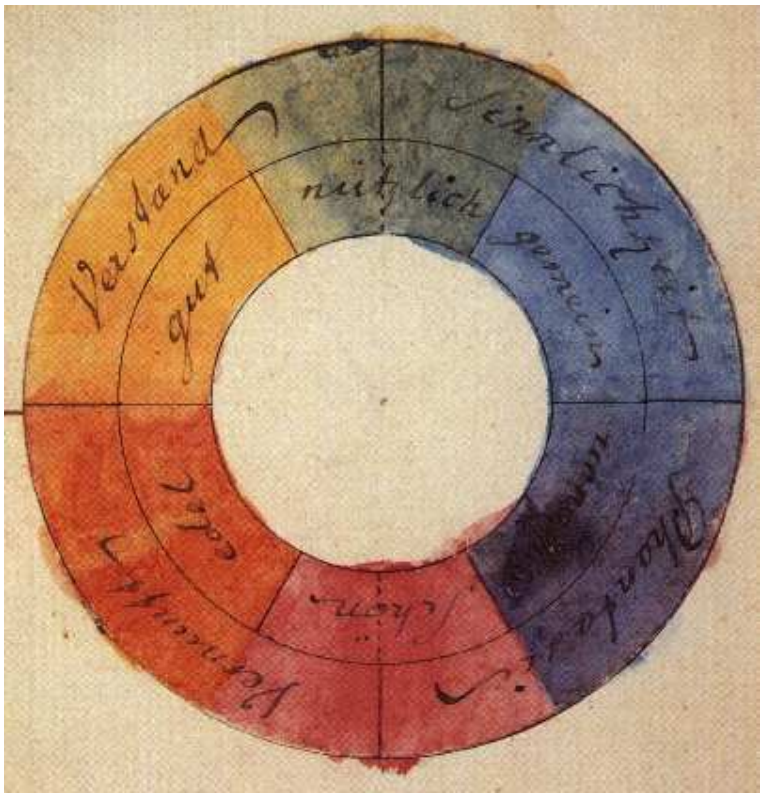

Figure 2.3: *Goethe's color circle.*

from the dynamic interaction between darkness and light.

In this way, he was trying to include also all the historical experience of artists and painters in the use and interaction of pigments, completely ignored at that time, even if they were the first to consider color as a context-ruled sensation.

Ewald Hering

In 1874 Ewald Hering[47] criticized Helmholtz's proposal for color perception explanation. The starting point of his proposal was the long debated role of yellow in color theories: in Helmholtz's color system, yellow sensation is derived by a mixture of red and green, Hering instead stated that yellow was an elementary sensation, and that a mixture of red and green was not possible, because that two colors eliminate each other.

Hering's approach was more concerned to qualitative and psychological aspects of color relations rather than to a physical definition, and therefore in his theory he sug-

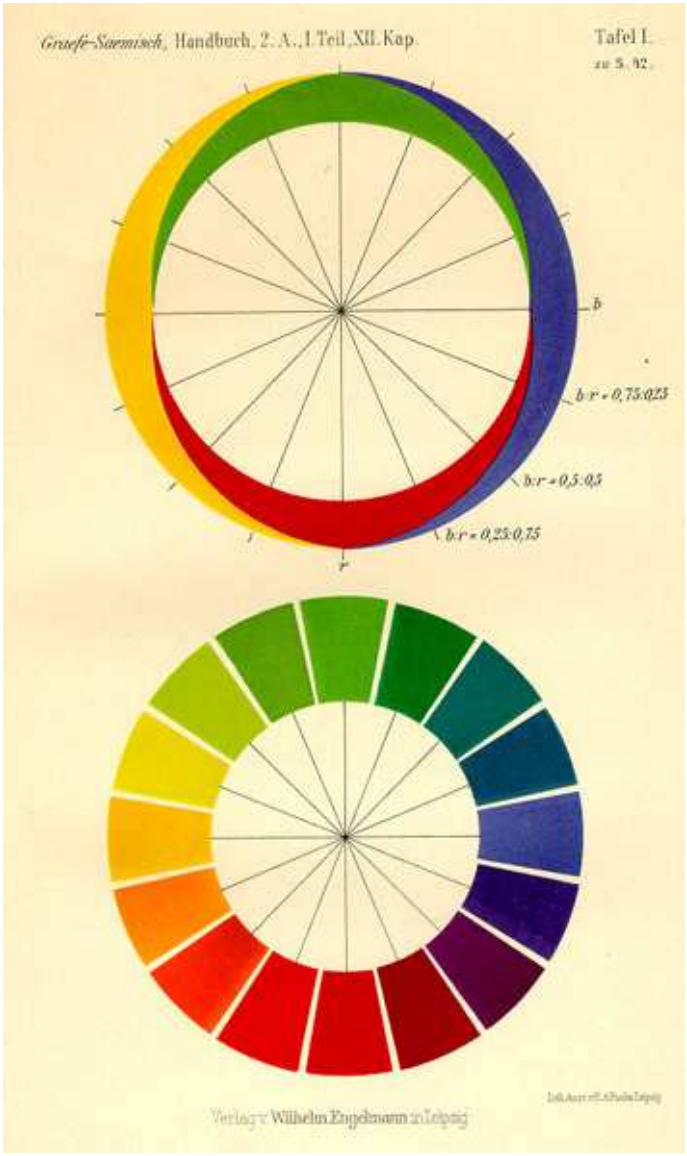

Figure 2.4: *Hering's opponent-colors system.*

gested that not three but four elementary sensations (called also *psychological primaries*) existed, coupled with the so-called *opponent processes*: any receptor that was turned off by one of these elementary sensations, was excited by its coupled color. He considered also white as an elementary sensation, not related to any mixture of basic colors, and therefore he suggested also the presence of another opponent process relative only to brightness.

In fig. 2.4 is shown his opponent-colors system, based on the red-green, yellow-blue

and white-black opponent processes.

Hering's proposal was hardly criticed by Helmholtz's theory supporters: they argued that his proposal could be acceptable only if two different and coupled processes of activation and inhibition existed in the nervous system. However, it is very remarhable how Hering's strictly empirical hypothesis has been demonstrated to be very coherent with the presence of opponent-colors neurons in the *lateral geniculate nucleus (LGN)*[127].

In his analysis of colors interaction, Hering noticed and analyzed color constancy phenomenon: however, he tried vaguely to explain it as the resulting effect of some not-well-defined physiological mechanisms, based on previous "memory" and "experience" of the observer, able to "discount the illuminant" of the scene[47,136].

Michel Eugène Chevreul

Even if not directly interested in art, Michel Eugène Chevreul had probably more influence on paintings development than other color scientists. His interest in color began in 1824, when, working on the chemical preparation of dyes for carpet production, he noticed that the color of the dyes appeared different when observed near other adjacent colors.

He decided to better investigate these effects, and in 1839 he proposed a detailed analysis of what are called *simultaneous contrast* phenomenons[13]. The basical observation was that looking at two colors side by side, one color lend its adjacent color a complementary tinge. The effect is most intense when the two colors are complementary colors.

Even if Leonardo da Vinci probably had been the first to notice the mutual influence of colors, and even if only some decades before his proposal Goethe had studied and proposed the relevance of these color interactions, Chevreul was the first to propose precise laws of color contrast, on which he elaborated a systematic organisation of colors (see fig. 2.5).

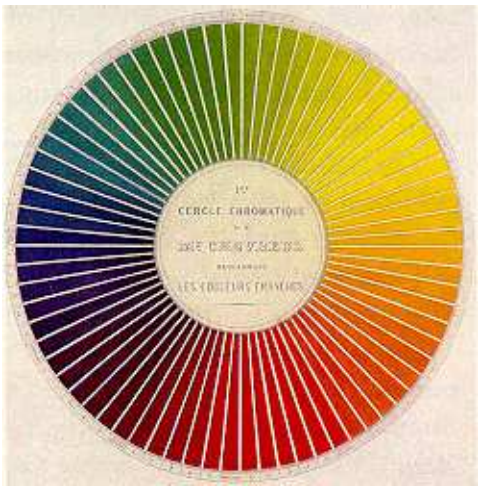

Figure 2.5: *Chevreul's color circle.*

2.2 Psychophysical experiments about color constancy

In the previous section we have summarized the two parallel approaches of color research in history. During the 20^{th} century, with the growing interest in a deeper understanding of color perception mechanisms, due also to the the availability of more details regarding the different areas of the brain and their roles, interesting psycophysical experiments have been proposed in order to better investigate color constancy phenomenon from a different point of view, less correlated to the spectral characterization of the light reflected from the observed objects, but more focused on the subjective processing of the incoming stimuli. Some of these experiments led to interesting hypothesis and theories about the effective nature of color constancy.

However we begin proposing two older experiments at first, contemporary to the previously presented theories, that shows how some remarkable efforts had been already done in investigating the real nature of color sensation, even if many physical and biological details about vision processes were unknown. We then present more recent and complete proposals of experimental setups, that investigate in robust and efficient way color constancy phenomenon.

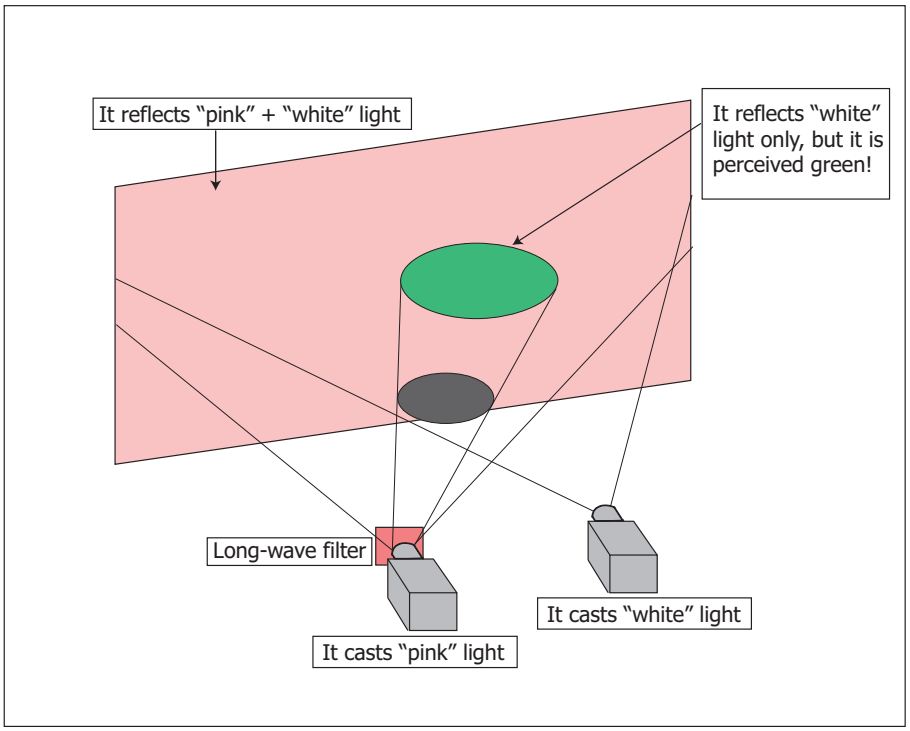

Figure 2.6: *Scheme of the colored shadow experiment using projectors.*

2.2.1 Colored shadows

First of all, we want to recall the so-called "phenomenon of coloured shadows". These phenomenon has been presented by Goethe[43] (there are also some studies in Leonardo Da Vinci's notebooks). The experiment can be easily replicated today illuminating a screen with two projectors, one casting white light, the other filtered with a not-too-peaked long wave pass filter, so to perceive a uniform pale pink observing the screen. Introducing an object in front of the filtered projector, we obtain a shadow on the screen that appears vivid green, despite the fact that the shadow area is physically illuminated only by white light (see the scheme in fig. 2.6).

2.2.2 Monge's experiment

In 1789 Gaspard Monge[77] proposed an experiment to demonstrate that color can not be described and defined only considering the nature of light incoming to the retina,

but that some perceptual process based on the analysis of the surrounding exists. He attached a sheet of red paper on a wall of a house. Then he invited the observers to look through a red glass and to analyze the color of the paper. Following the accepted theories about color, looking at a red paper through a red glass would have had to result in a red sensation, however the observers reported that the paper appeared whitish.

From this experiment, and considering also the phenomenon of colored shadows, Monge suggested that our visual system makes an estimation of the illuminant from the averaged spectral flux in the surrounding field of the observed object, applying then a cromatic correction. Even if currently it is proved that the HVS performs color constancy without any information regarding the illuminants, this approach (very remarkable considering the scientific knowledge regarding vision processes in Monge's historical period) is currently very considered by many scientists in the design and implementation of computional models of *machine* color constancy.

2.2.3 Land and McCann's experiments

However, probably the most famous experiments regarding color constancy are those proposed by Edwin Land and John McCann[66,63] in 1960-1970, and that represent the basis of the well-known *Retinex theory of color vision*.

In their first experiment they projected two black and white images of a scene: the first image was acquired using a long-wave pass filter, while a middle-wave pass filter was used for the second image. The first image was then projected using another long-wave pass filter in front of the equipment, while the second image was projected without filters, but using white light. Despite any expectation, the projected image presented a full gamut of colors and not simply white-pink shades.

Literature reports that, like most scientific discoveries, this important result was originally generated by an occasional event: Land was experimenting using three filtered projectors (one with long-wave, one with middle-wave, one with short-wave pass filter) to display three achromatic images acquired using a corresponding pass filter. "Short wave" projector was shut down, because he is investigating the lack of short wavelenghts in

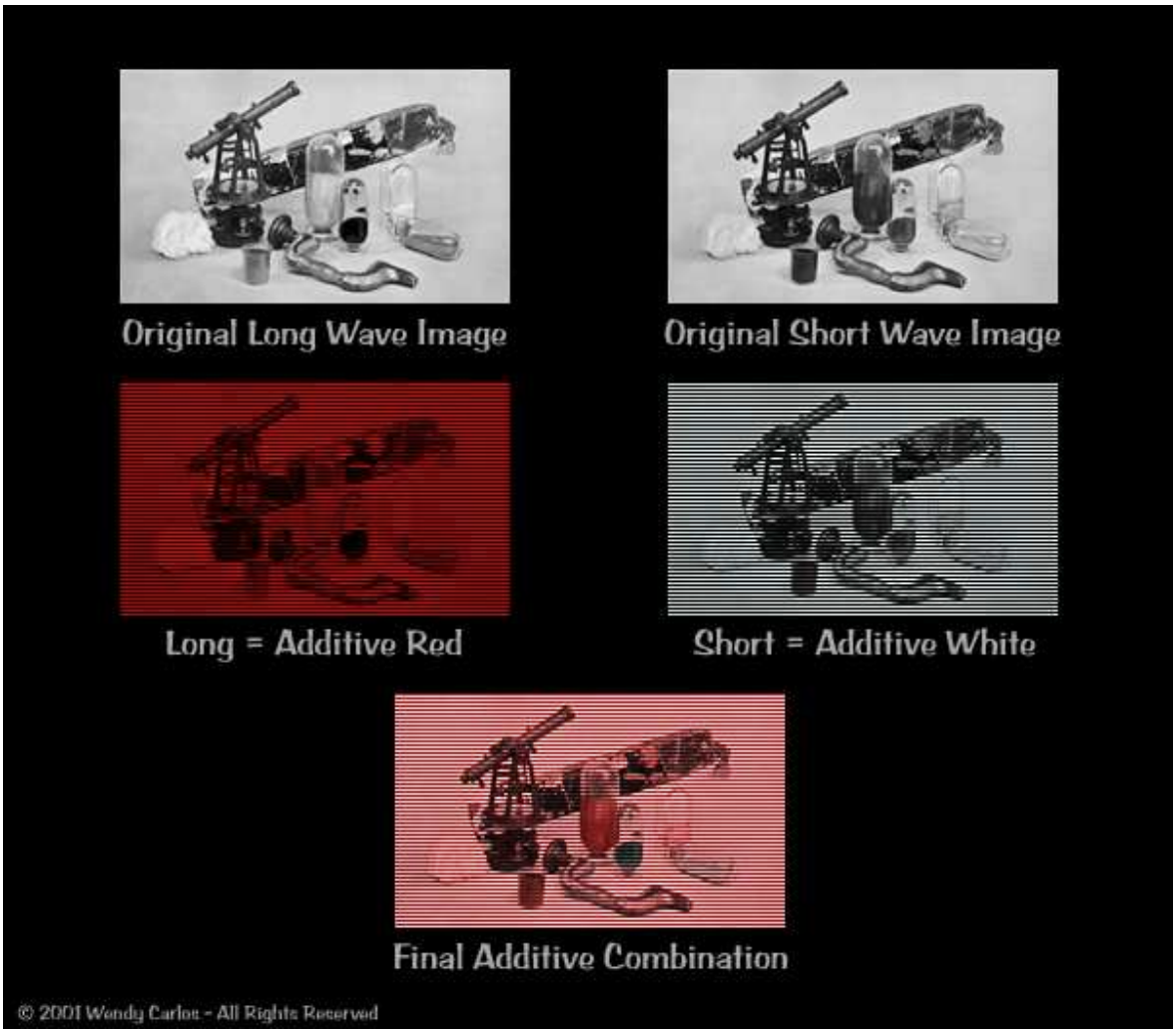

Figure 2.7: *An electronic reproduction of the first Land and McCann's experiment. The resolution of the final result here presented is not the most adequate to eliminate the stripes effect and to fully display the desidered effect, but however still is remarkable the green-blue shade of the object on the lower right. Original image courtesy of Wendy Carlos.*

spectral composition of light typical of sunrise. Somehow, some of his assistant removed the middle-wave pass filter from projector, leading him to that astonishing result.

In fig. 2.7 is presented an electronic reproduction of the experiment: the original black and white images have been manipulated with a image processing software in order to represent two interlaced frames, applying also a red filter to the first image.

Figure 2.8: *The setup of Mondrian experiments.*

Combining the two frames, working at a good resolution and looking at the result at some distance from the screen, we can obtain a good simulation, even if quite desaturated, of the original effect.

In their second experiment Land and McCann used a panel made of diffusive patches of paper of different colors, that they called "Mondrian", due to the resemblance with the paintings of the famous Dutch artist Piet Mondrian. The rectangular and square shapes of the patches avoided any form of recognition, while in the setup of the Mondrian particular care was taken to not surround a patch with another of a single color, so to avoid color induction effect.

The Mondrian was illuminated by three projectors, equipped with long-wave, middle-wave, short-wave pass filters and whose emitted light was adjustable using rheostats. A spectrometer was used to measure the spectral composition of light reflected by each

patch of the panel. In fig. 2.8 is shown the experimental setup.

During the experiment they adjusted the projectors light intensities in order to have the reflected light from a green patch characterized by a long wavelength dominant, and then asked the chosen observers to report the color of the patch. The observers reported the color to be green instead of red, as traditional color theories would suggest. The experiment was next repeated with a blue patch, adjusting the projectors so to have reflected the same spectral distribution as before. Again the observers reported the color of the patch to be blue.

Repeating the experiments with the two patches, but this time not viewed in the context of the Mondrian setup, but in *void conditions*, the observers reported the color of the patches to be white or light grey.

Starting from the impressive results of these experiments, Land and McCann concluded that the color of an object is determined not only by the wavelength dominant of the light reflected from it, but that is determined by comparing it with the spectral composition of the light reflected by the surrounding surfaces.

In their theory three separate channels, whose spectral sensitivities collide approximately with the cone responses, build a separate *lightness* record of the observed scene applying comparisons between reflected light from different surfaces, regardless of the spectral composition of the illuminants. The three independent records are then merged to form the final color sensation. They called their theory *Retinex* from *Retina* and *Cortex*, because they thought that both of them were involved in this processing.

Retinex theory became rapidly very popular in the scientific community, but it was also source of many discussions and criticisms: some scholars simply did not agree with Land's conclusions, others declared that color constancy phenomenon was already known and addressed by scientists with experiments and theories before Land and McCann's researches. In conclusion, they stated that Land was not giving such an innovative contribution, and that too much publicity has been given to the Retinex theory regarding the other approaches.

However, the historical theories for color vision before Land and McCann's proposal

were strictly related with the classical assumption that color is directly determined by the spectral characterization of reflected light, considering color constancy phenomenon simply as some sort of subsidiary, not well defined and surely not principal mechanism.

The innovative suggestion proposed by Retinex theory is that *color is an interpretation of the brain* of certain physical properties (the spectral characteristics of the reflected light from the observed surfaces), strictly related to the context of vision rather than based on the analysis of an isolated spectral stimulus. Using a definition by Zeki[136], with the proposal of Retinex theory finally *"Colour becomes a property of the brain"*.

Moreover, another relevant reason of the popularity of Retinex has been the specific intention from its authors to formulate a theory directly applicable in computational models, while other researches regarding color constancy theories or experiments have been proposed as "stand-alone" contributions without a pratical application. In chapter 3 Retinex-based computational models will be discussed.

2.2.4 Asymmetric Color-Matching experiments

During the 20^{th} century, two kinds of asymmetric color-matching experiments[127] were used to measure and analyze cone absorptions induced by incoming lights from objects with same color appearance under different illuminants.

The first is known as *memory-matching* method: in this experiment the observer studies the color of a target presented under an illuminant and then he must select a new target with the same appereance under a different illumination.

The second is called *dichoptic matching* method: in this case the observer views simultaneosly a different scene in each eye, one exposed to a uniform background illuminated by daylight lamp, the other to an equivalent background but illuminated by tungsten lamp. A target stimulus is placed at the center of one of the backgrounds, and the observer has to select an object with the same appearance from a set of possible targets seen under the other configuration.

These experiments were used mainly to test and discuss the *coefficient law* proposed in 1905 by Von Kries[125], rather than investigating new hypothesis regarding color con-

stancy mechanisms. Therefore, these researches did not contribute in a remarkable way in the development of new computational models.

In his theory, Von Kries suggested that a linear adjusting of the sensitivity of the three photoreceptors occurs independently in proportion to their responses at spectral variations of the incoming light. As example, we recall the experimental tests performed by Wassef[130] in 1959.

2.2.5 Brainard and Wandell's experiment

In 1992 Brainard and Wandell[5] used a slightly different memory-matching method in order to evaluate how well perceptual mechanisms correct illumination changes (i.e. the correctness of our color constancy).

They presented to the observers on a display virtual patches rendered with computer graphics techniques simulating daylight illumination. The observers had to memorize the appereance of a surface. Then the simulated illuminant was changed slowly, over a period of two minutes, in order to let the subjects to adapt to the new illuminant. Then they were asked to adjust the appearance of another virtual surface on the basis of the precedent memorized sensation.

Analyzing the obtained results, the conclusion was that the observers estimated in their choices a smaller illumination changes than the real introduced variation: quantitatively, their correction was about half the true illuminant change.

2.3 Computational models of color in context

In some sense, in this chapter we are presenting a brief description of the main stages of color research. We have discussed the historical approaches, characterized by the first, often empirical, assumptions, without physiological nor technological knowledges, but simply based on the observation of experiments and on deduction, that during the years have evolved into the modern colorimetry. Then we have presented the psychophysical efforts in the understanding of perceptual mechanisms, based on the

continuos discoveries about brain physiology and the theories about the cortical areas involved in color sensation.

With the introduction and the availability of calculators, we can identify the third stage in the growing interest in a correct computational reproduction of color and in the simulation of color perception mechanisms by the development of algorithms.

In the last decades, many computational models for image processing applications based on color computation have been proposed, each differing for the underlying approach. Some of them try to simulate in details recent discoveries regarding inner neural mechanisms of the brain, others instead simply consider and implement macro-behaviors of the HVS.

We will give a brief description of the main approaches used in the image processing field, suggesting some examples for each category, following partially a classification proposed by Gatta[40].

Many simple algorithms have been proposed based on Von Kries hypothesis[125] (see subsection 2.2.4): these models apply a global linear scaling independently on the three chromatic channels on the basis of the brightest value found in each channel. This approach is not perceptually correct, because it does not consider contextual mechanisms of color vision, and computationally it clearly fails in presence of a single bright (or noisy) pixel. However in slightly modified versions it is the most used approach for color correction mechanisms embedded in digital cameras, due to its high computational efficiency.

Other computational models follow the so-called *gray-world* assumption, i.e. that the average surface reflectance of objects in a scene corresponds to gray. Following this hypothesis, illuminant characteristics can be detected calculating the shift between the average value of pixels in the input image and the assumed gray value, and then used in the color correction stage. This kind of algorithms has been introduced by Buchsbaum in 1980[9], and some modified versions have been proposed in the following years.

A more sophisticated group of algorithms addresses color constancy problem by estimating and then discounting the illuminant of the scene. These models are mainly

statistical methods based on data fitting or correlation. For example, in the Color-by-Correlation algorithm, proposed in 2001 by Finlayson et al.[36], a set of possible lights are chosen. Then it is determined which colors can occur using each of these possible lights and how they are distributed, and a *correlation matrix* is constructed. After this pre-processing stage, the colors in a input image are compared with the correlation matrix values, in order to measure the probability that one of the possible lights chosen in the first stage could be the unknown illuminant in the image. In the final stage, probabilities are analyzed in order to choose one of the chosen light as an estimate of the scene illuminant.

However, this kind of approach is more concerned with so-called *machine color constancy*, i.e. the ability of some algorithms to extract the reflectance property of objects removing the illuminant, rather than *human color constancy*, that acts without any illuminant estimation and taking inspiration by human perception mechanisms, like e.g. Retinex computational models.

In this dissertation we propose new Retinex-based computational models for image processing and computer graphics applications, therefore we will address Retinex algorithms in more details in chapter 3.

The previously cited algorithms have been implemented with the intent to have a high level approximation of the mechanisms of color perception, starting from the results of psychophysical researches, rather than accurately implement each neural mechanism.

However, other very complex computational models have been proposed trying to simulate in details the different stages of color signal processing in the various cortical areas of the brain, from cone responses in the retina to the opponent signals generation in lateral geniculate nucleus, until the spatial processing in cortical area V4.

Examples of this kind of computational models, often characterized by a neural network approach, have been proposed by Moore et al. in 1991[78], by Courtney et al. in 1995[22], by Ross and Mingolla in 1998[100] and more recently by Spitzer and Semo in 2002[107].

Chapter 3

Retinex computational models

Contents

Since its proposal in 1971[66] by Edwin Land and John McCann, the Retinex model is widely used as a starting point for new computational models of color sensation. These models have some common points with the original Retinex algorithm[66,63] but most of them add or modify the basic principles of the algorithm.

There are some interesting papers that describe Retinex and some modified versions[3,4,70,95,38,53], the analysis and tuning of its parameters[18], and some works investigating the application of Retinex in new fields of computer graphics like tone mapping[104,39,99] or spatial gamut mapping[74]. Application of Retinex in the tone mapping field will be addressed in chapter 4.

In this chapter, after a short description of the original Retinex algorithm, we present a rigorous mathematical definition and analysis[89] of Retinex theory. Finally a new implementation called "Random Spray Retinex", in which paths are replaced by 2-dimensional pixel sprays, is proposed.

3.1 The Retinex algorithm

The Retinex theory assumes that human vision is based on three retinal cortical systems, each independently processing the signals produced by l, m and s cones. Each independent process forms a separate image determining the relative lightness values of the various regions of a scene[63] (see subsection 2.2.3 for details).

Biological studies show that there's a lack in this theory: if we look at the post-retinal computation, we found explicit connection between different cone responses[136]. However, the Retinex algorithm is not a biological simulation of the color sensation process. The l, m and s cones are usually approximated using R, G and B values obtained by digital devices.

According to Land and McCann, edges between adjacent areas of an image play a fundamental role in color perception. Therefore, the ratio of lightness between two areas has been chosen as a dimensionless property describing their relationship. If these two

areas have lightness which are very different, the ratio is far from the unitary value, and it tends toward the value of 1 where the lightness tend to become equal. If the ratio is computed and averaged in many locations of the image, Retinex can discounts a possible chromatic cast and dimensionless character of computation will help to equalize the overall lightness of the image.

The visual response S^x at the location x of the image is:

$$S^x_{R,G,B} = \int_{\lambda \in (400nm, 700nm)} E(\lambda) R^x(\lambda) \rho_{R,G,B}(\lambda) d\lambda \tag{3.1}$$

where x is a discrete spatial coordinate, $E(\lambda)$ is the spectral power distribution of the illuminant light, $R^x(\lambda)$ is the reflectance at the point x and $\rho_{R,G,B}$ is the spectral sensitivity of the photoreceptor's (retinal cones) pigment. The relative lightness $L^{i,j}_{R,G,B}$ at point x, along a path in the image (Fig. 3.1), for each channel RGB, is computed in the following way:

$$L^{i,j}_{R,G,B} = \sum_{x \in path} \delta(\log(S^{x+1}) - \log(S^x)) \tag{3.2}$$

where

$$\delta = \begin{cases} 1, & \text{if} \quad |\log(S^{x+1}) - \log(S^x)| > threshold \\ 0, & otherwise \end{cases} \tag{3.3}$$

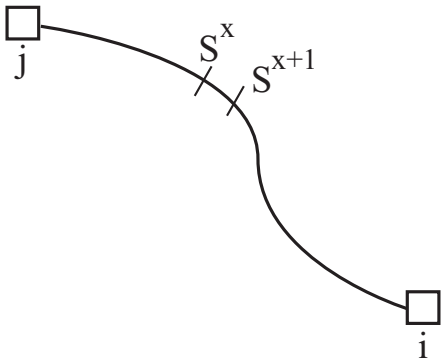

Figure 3.1: *Along the path from point j to point i, the relative lightness is computed as the ratio between the visual responses at the generic points x and $x+1$.*

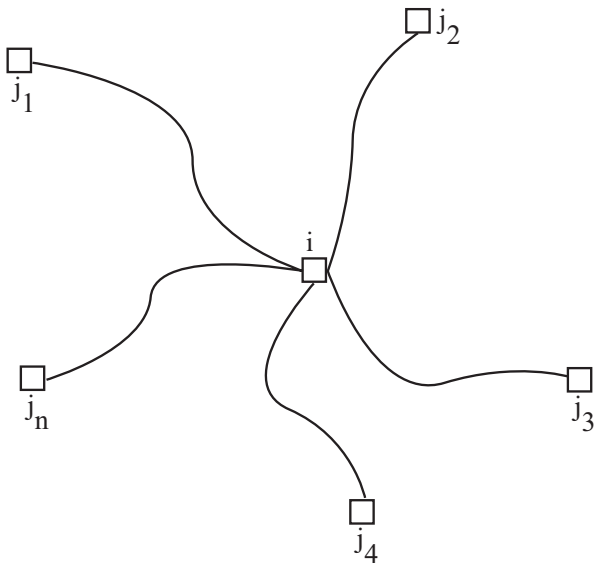

Figure 3.2: *Example of paths from points $J_1, J_2, \ldots, J_n$ for the computation of the lightness value at point i.*

Hence, the calculated RGB intensity value for each point i is the mean value of relative lightness $L^{i,j}_{R,G,B}$ computed over a number N of paths ending at point i (Fig. 3.2):

$$L^{i}_{R,G,B} = \frac{\sum_{k=1}^{N} L^{i,j_k}_{R,G,B}}{N} \tag{3.4}$$

These computations must be executed separately for the three channels RGB.

The model above depends on the number of the chosen paths, and on the *threshold* value that makes it possible to disregard low lightness ratios, which correspond to smooth changes in color due to non-uniform illumination.

The Retinex algorithm has a *reset* mechanism by means of which, during a path computation, if a lighter area is found, the cumulated relative lightness is forced to the unitary value, making the average computation restart from this area. The effect of the reset mechanism is to consider the lightest area of an image as a local reference value for white.

The reset process is responsible of the *white patch* behavior of the Retinex algorithm. Without the reset, Retinex cannot have a reference during the computation.

This process is highly non linear since it turns to 1 the computed ratios on the *path* if the cumulated product is greater than 1. In[73] we can found the importance of a non linear operator to predict simultaneous contrast configurations.

Retinex models[66,65] compute the lightness of each pixel in the image using data collected from other pixels. These models incorporate the concept of locality by gaining the data to compute lightness in a local way, i.e. considering the data close to the computed pixel and not an averaged value of the whole data representing the input image. A description of different ways of exploiting locality is shown in section 3.2.

3.2 Sampling vs Integrating

The Retinex computation is strongly related on the concept of spatial color. Spatial color means that the color *appearance* of an area (or object) is related to the context. The context is simply the color distribution around an area.

All Retinex algorithms exploit locality. There are two different ways used for giving locality to the algorithm:

- *Sampling*: The algorithm samples values in the image using different methods: Brownian paths[69], spiral paths[37,38] or double spiral paths[19].
- *Integrating*: The algorithm gain information on context by an averaged value of the data in the surround. The average could be computed using a weighting function.[65] and its derivations[53,54,3] are two examples of this method.

These two methods are very different. The Retinex formulation of[65] is described by the following formula:

$$R_c(x,y) = \log(I_c(x,y)) - log(F(x,y) * I_c(x,y)) \tag{3.5}$$

where I is the input image, $c = \{R, G, B\}$, and $F(x,y)$ is the surround function. It is important to note that for every pixel only one comparison is made between the pixel value and the integrated value over the surround function.

Moreover the convolution process gives a weighted average value of the neighborhoods to summarize the surround contributions to the lightness of the target pixel. This is different from others Retinex models that sample the image with paths that travels the image.

However, the integrating method has the disadvantage of summarizing in a single value the spatial distribution of the surround: this is a critical point and the source of the major drawbacks of integrating-based Retinex implementations.

In fact using a small surround leads to a significant increase in local contrast but induces halo artifacts along high contrast edges and an overall effect of desaturation in final color rendition. However, adopting a larger surround reduces the artifacts, but provides less increase in local contrast.

The limitation of the *integrating* method is overcome in a work proposed by Meylan and Süsstrunk in 2006[76]: the authors determine the surround using an adaptive filter whose shape follows the image high contrast edges.

3.3 Three examples of Retinex-based computational models

As previously said, many Retinex-based computational models have been proposed. In this section we briefly present three algorithms: the Brownian Retinex proposed by Marini and Rizzi[69], the Multilevel Retinex proposed by John McCann[74], and the Automatic Color Equalization (ACE) algorithm from Rizzi et al.[97] The first two operators represent two different approaches in the application of Retinex theory, when ACE otherwise is a new model implemented on the common assumptions of Retinex theory, but reimplementing them in different ways.

Figure 3.3: *Example of 10 Brownian paths.*

3.3.1 Brownian Retinex

In 2000, Marini and Rizzi[69] proposed a Retinex implementation called *Brownian Retinex*.

This implementation is characterized by the construction of Brownian random paths (see fig. 3.3) in the image, inspired by the distribution of receptive field centroids in cortical area V4[136], responsible for color vision in complex scenes.

The approximation method used to construct the random paths is the well-known mid-point displacement recursive algorithm[102], that displaces randomly the middle point of a segment and applies recursively the same method on the new two generated segments.

Along each path, the algorithm scan converts the pixels, computing the relative reflectance for each pixel along the edge applying the Retinex mechanisms illustrated in section 3.1.

A relevant effect of the application of random paths was the need of a smaller number of paths than the other Retinex implementations in order to approximate the lightness value of each pixel.

The authors tested the color correction effect of the algorithm applying chromatic distances in CIELAB space on a set of synthetic images rendered using various standard illuminants. Moreover, they verified the ability of the computational model to simulate perceptual rensponse applying the algorithm to some classical color illusions.

3.3.2 McCann Multilevel Retinex

The Multilevel Retinex proposed in 1999 by John McCann[74,38] is characterized by the construction of a multiresolution pyramid from the input image by averaging image data.

For all levels, beginning at the top level of the pyramid, the new product for each pixel is computed by applying ratio-product-reset mechanisms to each of its eight immediately neighboring pixels in clockwise order.

After computing lightness on the image at a reduced resolution, the resulting lightness values are propagated down, by pixel replication, to the next level of the pyramid as its initial lightness estimates. This process continues until new products have been computed for the pyramid's bottom level.

A crucial parameter of the algorithm is the number of times a pixel's neighbors must be visited. It is equivalent to set the distance at which pixels influence one another: in fact, the new product values for all pixels are computed in parallel, so, after one iteration, all neighboring pixels have had their new products values updated. Therefore, the number of iterations is a crucial parameter in order to have a correct computation of local and global effects in the output results.

A proposal for an automatic determination of this parameter has been addressed by Ciurea and Funt in 2004[18].

3.3.3 Automatic Color Equalization (ACE)

The Automatic Color Equalization (ACE), proposed by Rizzi et al.[97] in 2003, maintains the main Retinex idea that the color sensation derives from the comparison of the spectral lightness values across the image, but also it considers the lightness constancy mechanism, i.e. the ability of our visual system to make us perceive as medium gray the objects which reflect the average luminance of a scene.

The algorithm is subdivided in two parts: in fig. 3.4 is represented the scheme of the computational model. The first part of the model performs a spatial variant

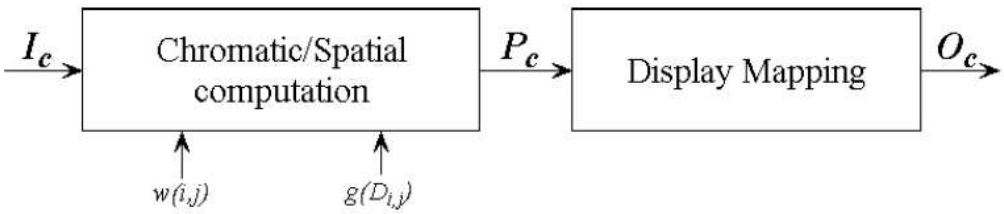

Figure 3.4: *Scheme of ACE algorithm.*

computation and the second performs a spatial invariant display mapping.

Chromatic/Spatial computation

Tha mathematical definition of the first part of the ACE algorithm is defined in equation 3.6:

$$P_c(i) = \frac{1}{k_i} \sum_{j \in I \setminus \{i\}} g(I_c(i) - I_c(j)) w(i,j) \tag{3.6}$$

where k_i is a normalization factor defined as:

$$k_i = \sum_{j \in I \setminus \{i\}} w(i,j) \tag{3.7}$$

In ACE algorithm each pixel is compared to every other in the input image I: the pixel to pixel comparison is made by arithmetical difference, and this difference is modified by the non linear function g, that computes lightness between two pixels value. This function (shown in fig. 3.5) acts as the non linear *reset* mechanism of the original Retinex algorithm, but is able to simulate also the lightness constancy mechanism.

The combination of the difference and of the non linear function g can achieve a behavior that is comparable to the ratio-reset of Retinex algorithms.

To modify the influence between close and distant pixels in Retinex algorithms, paths or center/surround approaches are considered. Differently, ACE implements spatial computation applying a distance function w to every comparison. The authors tested *Euclidean*, *Inverse exponential*, *Manhattan* and *Maximum* distances, and in the end

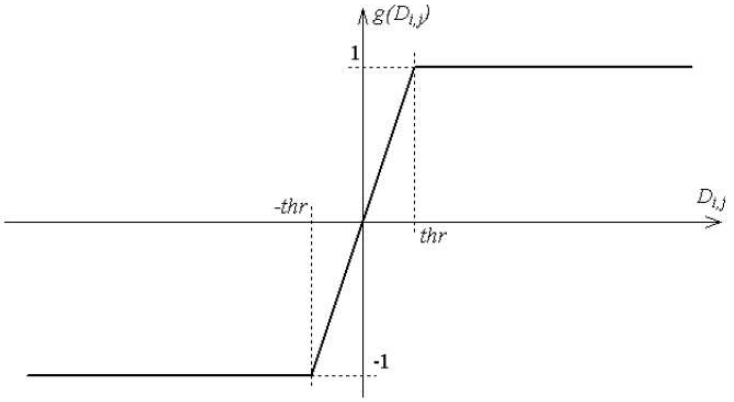

Figure 3.5: *Graph of $g(D_{i,j})$ function, where $D_{i,j} = I_c(i) - I_c(j)$.*

they adopted the inverse of the Euclidean distance because it performed better in their experiments.

Display mapping

To display the computed values into the available display dynamic range the authors tested two different solutions.

The first is a simple linear scaling of the values of intermediate image P_c (the output of the first stage of the algorithm) into the output result O_c. This is done independently in every chromatic channel c.

The alternative and more satisfactory method uses the maximum value in each chromatic channel as white reference, and the zero value in P_c as an estimate for the medium gray reference point to compute a linear mapping function that makes the dynamic of the final image to be always centered around the medium gray.

3.4 Mathematical analysis of the Retinex algorithm

In[89], authors describe mathematically the Retinex algorithm of Land and McCann[66]. The Retinex algorithm depends on some parameters (such as threshold, number of paths and iterations). The authors show that the qualitative behavior of Reti-

nex in relation with the variation of these parameters can be predicted by using the mathematical definition.

Given a digital image, consider a collection of N oriented paths γ_k composed by ordered chains of pixels starting in j_k and ending in i. Let n_k be the number of pixels travelled by the path γ_k and let $t_k = 1, \ldots, n_k$ be its parameter, i.e. $\gamma_k : \{1, \ldots, n_k\} \to I\mathit{mage} \subset \mathbb{R}^2$, $\gamma_k(1) = j_k$ and $\gamma_k(n_k) = i$.

Write, for simplicity, two subsequent pixels of the path as $\gamma_k(t_k) = x_{t_k}$ and $\gamma_k(t_k + 1) = x_{t_k+1}$, for $t_k = 1, \ldots, n_k - 1$. Consider, in every fixed chromatic channel $c \in \{R, G, B\}$, their intensities $I(x_{t_k})$, $I(x_{t_k+1})$ and then compute the ratio $R_{t_k} = \frac{I(x_{t_k+1})}{I(x_{t_k})}$. For technical reasons put $R_0 = 1$ and normalize the intensities to take their values in the real unit interval (the normalization factor is $\frac{1}{255}$ if 8 bits are used for each pixel in every chromatic channel).

The (normalized) value of lightness given by Retinex for a generic pixel i, in every fixed chromatic channel c, can be obtained by this formula:

$$L(i) = \frac{1}{N} \sum_{k=1}^{N} \prod_{t_k=1}^{n_k-1} \delta_k(R_{t_k}) \tag{3.8}$$

where $\delta_k : \mathbb{R}^+ \to \mathbb{R}^+$, $k = 1, \ldots, N$, are functions defined in this way: $\delta_k(R_0) = 1$ and, for $t_k = 1, \ldots, n_k - 1$,

$$\delta_k(R_{t_k}) = \begin{cases} R_{t_k} & \text{if } \ 0 < R_{t_k} \leq 1 - \varepsilon \\ 1 & \text{if } \ 1 - \varepsilon < R_{t_k} < 1 + \varepsilon \\ R_{t_k} & \text{if } \ 1 + \varepsilon \leq R_{t_k} \leq \frac{1+\varepsilon}{\prod_{m_k=0}^{t_k-1} \delta_k(R_{m_k})} \\ \frac{1}{\prod_{m_k=0}^{t_k-1} \delta_k(R_{m_k})} & \text{if } \ R_{t_k} > \frac{1+\varepsilon}{\prod_{m_k=0}^{t_k-1} \delta_k(R_{m_k})} \end{cases}$$

being $\varepsilon > 0$ a fixed *threshold*.

It is useful to write *the contribution of the single path* γ_k *to* $L(i)$ as: $L_k(i) = \prod_{t_k=1}^{n_k-1} \delta_k(R_{t_k})$, so that formula (3.8) reduces simply to the average of these contributions: $L(i) = \frac{1}{N} \sum_{k=1}^{N} L_k(i)$.

In[89] can be found the proof that this mathematical formulation is equivalent to the algorithm described by Land and McCann. They also note that the threshold mechanism

makes hard to predict mathematically some properties of Retinex. Thus they decide to remove the threshold mechanism showing that it does not influence heavily the final result.

They introduce the new formula setting $\varepsilon = 0$:

$$\delta_k(R_{t_k}) = \begin{cases} R_{t_k} & \text{if } 0 < R_{t_k} \cdot \prod_{m_k=0}^{t_k-1} \delta_k(R_{m_k}) \leq 1 \\ \frac{1}{\prod_{m_k=0}^{t_k-1} \delta_k(R_{m_k})} & \text{if } R_{t_k} \cdot \prod_{m_k=0}^{t_k-1} \delta_k(R_{m_k}) > 1 \end{cases}$$

hence δ_k, when the threshold is 0, behaves like the identity function or like the reset function.

They show that, *when $\varepsilon = 0$ all the pixels travelled by the path γ before the pixel with highest intensity are perfectly uninfluential for the computation of $L(i)$*. Thus they point out that only the maximum value x_{H_k} is important for the computation.

Thanks to these properties, and considering that $I(i)$ is independent from k, they formulate a very compact mathematical description of Retinex:

$$L(i) = I(i) \cdot \frac{1}{N} \sum_{k=1}^{N} \frac{1}{I(x_{H_k})} \tag{3.9}$$

which shows explicitly that, at a mathematical level, Retinex without threshold acts on the intensity of each pixel as a multiplication operator, with the multiplicative factor given by the average of the inverse values of the highest intensities of the pixels travelled by the paths γ_k.

An important proof is that, recalling that the intensity values are normalized, so $0 < I(x_{H_k}) \leq 1$ for every $k = 1, \ldots, N$ and then $\sum_{k=1}^{N} \frac{1}{I(x_{H_k})} \geq N$. It follows that $L(i) \geq I(i)$ for every pixel i and this is a rigorous proof of the fact that *an image filtered with Retinex without threshold is always brighter or equal to the original one.*

With the help of the formula (3.9) they prove that if an image is filtered many times with Retinex without threshold, then it converges to an image characterizable in a simple way: the image of convergence is obtained when *the lightness of (at least) one pixel in all the paths $\gamma_1, \ldots, \gamma_N$ reaches the value 1.*

They shows that when $N \to \infty$, where N is the number of the paths that scan the image, the Retinex behaves like a global White Patch algorithm. This is very important since this fact shows that the locality of the algorithm is very important to the final goal.

3.5 Random Spray Retinex (RSR)

In order to investigate the local filtering behavior of the Retinex model, we propose a new implementation in which paths are replaced by 2-dimensional pixel sprays, so the name *Random Spray Retinex*[90]. A peculiar feature of this implementation is the way its parameters can be controlled to perform spatial investigation. The parameters tuning is accomplished by an unsupervised method based on quantitative measures. This procedure has been validated via user panel tests. Furthermore, the spray approach has faster performances than the path-wise one. Tests and results are presented and discussed.

In the basic Land and McCann implementation of Retinex, locality is achieved through paths scanning images.

All the sampling implementations that use a path-wise approach have to deal with the following problems: strong dependency on paths geometry, high computational cost and sampling noise.

On the basis of the mathematical analysis of path-wise Retinex algorithms[89] described in section 3.4 we will prove the intrinsic redundancy of this approach. Consequently, we will propose an extension that allows to keep the sampling approach highly reducing the typical problems related to the use of paths.

This alternative technique is constructed replacing paths with random sprays, i.e. two-dimensional point distributions across the image, so the name *Random Spray Retinex (RSR)*[90]. We will show how it is possible to change the spray density around a pixel and how this leads to the ability of finding out information about locality of color perception within the Retinex model.

3.5.1 From paths to pixel sprays

The information given by the mathematical formulation of Retinex have strong consequences on the structure of $\mathcal{P}_i(Image)$: the set of paths embedded in the image and *ending in the point* i. After formula (3.9), on this set it is natural to define this equivalence relation: given $\gamma, \eta \in \mathcal{P}_i(Image)$,

$$\gamma \sim \eta \quad \Leftrightarrow \quad \max_{(x,y)\in\gamma^*}\{I(x,y)\} = \max_{(x,y)\in\eta^*}\{I(x,y)\} \tag{3.10}$$

where γ^* and η^* are the codomain of the paths, i.e. the collections of pixels traveled by γ and η, respectively.

Paths belonging to different equivalence classes give different contributions to the lightness computation, while every path in a given equivalence class is characterized by the same value of $L_k(i)$. It immediately follows that, for the purposes of Retinex, $\mathcal{P}_i(Image)$ contains redundant paths and so the really interesting set of paths is the *quotient set* $\mathcal{P}_i(Image)/\sim$, whose elements are the equivalence classes of paths with respect to the equivalence relation defined in (3.10).

Thence path-wise Retinex implementations are affected by two kind of redundances: from one side many paths must be used to reduce the sampling noise; from the other side, as just proved, they can be organized in equivalence classes, so that if one uses two paths belonging to the same class they will lead to the same chromatic information, i.e. they are redundant.

In each equivalence class one can choose a single representative path to compute $L_k(i)$, in particular, the shortest one is the two-points path whose codomain is simply $\{x_{H_k}, i\}$. It follows that the ordering operations needed to generate the paths are perfectly uninfluential for the final lightness computation.

Moreover, by a mathematical point of view, paths are topological manifolds of dimension 1 embedded in the image, which is a topological manifold of dimension 2, so paths do not really scan local neighborhoods of a pixel, but rather *particular directions* in these neighborhoods. This directional extraction of information can lead to halos or artifacts in the filtered image.

The classical implementations of Retinex try to remedy this problem using a large number of paths, but this increases the filtering time and does not really overcome the problem.

We see that there are three reasons for which paths are not perfectly suitable for the analysis of locality of color perception within the Retinex model: they are redundant, their ordering is completely uninfluential and they have inadequate topological dimension.

Thus, we are lead to use 2-dimensional objects such as *areas* instead of 1-dimensional paths to analyze locality of color perception. More precisely, our idea is to implement the investigation about locality selecting pixels from these areas with a density sample that changes according to a given function of their distance with respect to the target pixel i. Each function generates a different kind of pixel selection around i, leading to different kind of "sprays", each of which reveals different local filtering properties.

3.5.2 RSR implementation

RSR is a new implementation of the original Retinex model[66] which has been inspired from the results of the mathematical analysis of Retinex[89] described in section 3.4. In RSR the role of a path γ_k traveling n_k pixels and *ending* in the target i is played by $Spray_k(i)$, a spray composed by n_k pixels and *centered* in i. In fact, N random sprays are selected from a pre-computed set (the symbol N now will be used to denote the number of sprays to put in stronger evidence the correspondence between paths and sprays).The typical ratio-reset operation along a path is substituted by the search of the pixel with highest intensity in the whole spray. It will be clear from the following discussion that, once the number of points per spray is chosen, there is no need to vary it with k, hence, from now on, we will write n instead of n_k to denote the number of pixels per spray.

The functional expression of the formula (3.9) to compute the lightness remains exactly the same in both algorithms, so they share the same intrinsic properties described in section 3.4. This is the reason why the results about locality of color perception that

we will get thanks to the RSR *implementation* can be referred to the Retinex *model*.

Notice that the only operations performed by RSR in each spray are n comparisons (needed to find out the pixel with highest intensity) and one division. So RSR is significatively faster than the previous path-wise Retinex implementations.

Let us now show how to construct $Spray_k(i)$. With a random point generator we can get a *uniform random distribution* of n values in the real unit interval $[0, 1]$. Then, by multiplication, we can extend this distribution to any real interval, in particular, we are interested to the intervals $[0, 2\pi]$ and $[0, R]$, where R is a given positive real number that will represent the radius of the spray. We denote, respectively, with $\text{RAND}_n[0, 2\pi]$ and $\text{RAND}_n[0, R]$ the corresponding uniform random distributions.

Now, if (i_x, i_y) are the coordinates of i, we can define the polar coordinates of a generic pixel $j \equiv (j_x, j_y)$ belonging to $Spray_k(i)$ in this way:

$$\begin{cases} j_x = i_x + \rho \cos(\theta) \\ j_y = i_y + \rho \sin(\theta) \end{cases} \tag{3.11}$$

where $\rho \in \text{RAND}_n[0, R]$, $\theta \in \text{RAND}_n[0, 2\pi]$.

These are the coordinates of pixels that have an isotropic angular distribution in a circle of radius R centered in the pixel i.

Notice, however, that the radial density is not isotropic, in fact, because of the rotation, the spray results more dense near the target pixel i than far away. We can easily compute the *average radial density* $\delta(r)$ considering, as in fig. 3.6, a circle C_r of arbitrary radius r, $0 < r < R$, centered in i and then taking the ratio between the number of points inside C_r and its area, i.e. $\delta(r) = dn/dA$.

The number of points inside C_r is $n(r) = n\frac{r}{R}$, since we are dealing with uniform random distributions.

Considering also that $A = \pi r^2$, and therefore $r = \sqrt{A/\pi}$ (since $r \geq 0$), we can express $\delta(r)$ as:

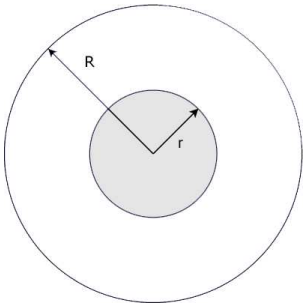

Figure 3.6: *Computation of the areolar density in function of the spray radius.*

$$\begin{aligned}\delta(r) &= \frac{dn}{dA} \\ &= \frac{d}{dA}\left(\frac{n}{R}\sqrt{\frac{A}{\pi}}\right) \\ &= \frac{n}{2R\sqrt{\pi A}} \\ &= \frac{n}{2\pi r R}\,.\end{aligned} \tag{3.12}$$

Thus the average radial density of spray pixels decreases as the inverse radius.

Fig. 3.7 shows an example of such a spray with 400 pixels and radius $R = 1$.

The angular isotropy is a natural requirement that must be satisfied by the spray, since the presence of privileged directions generates artifacts in the filtered image.

Now, the local properties of Retinex can be analyzed in a very simple way applying a function on the coordinate ρ to change the radial density of the spray pixels around i. Precisely, given any function $f : \mathbb{R}^+ \to \mathbb{R}^+$, we can consider the modified spray whose pixels have polar coordinates defined by:

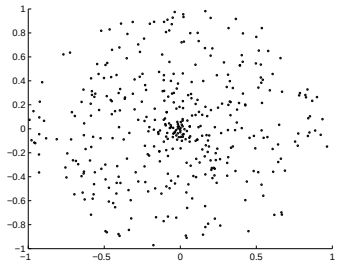

Figure 3.7: *An example of "naturally localized" spray.*

$$\begin{cases} x = x_i + f(\rho)\ \cos(\theta) \\ y = y_i + f(\rho)\ \sin(\theta) \end{cases} \tag{3.13}$$

where, again, $\rho \in \text{RAND}_n[0, R]$ and $\theta \in \text{RAND}_n[0, 2\pi]$. It is useful to distinguish the special case in which $f \equiv id_{\mathbb{R}^+}$, the identity function restricted on non-negative real numbers, calling the corresponding spray "naturally localized".

Figs. 3.8-3.11 show some examples of sprays with $R = 1$, $n = 400$, obtained with different functions f.

It can be seen that the normalized logarithmic and hyperbolic sinus functions keep the spray density quite similar to the one of the naturally localized spray. Instead powers of ρ with exponent greater than 1 and the normalized exponential function tend to increase the density around the center. Finally, powers of ρ with exponent in $(0, 1)$ and the normalized inverse exponential applied on ρ tend to delocalize the spray. The multiplication of ρ by a constant coefficient m simply changes the radial extension of the naturally localized spray, expanding the radius, when $m > 1$, or contracting it, when $0 < m < 1$.

To perform the analysis of locality in RSR we must tune f and the other parameters of the algorithm. Before showing the results about tuning, we briefly summarize all these parameters and discuss their meaning in the next subsection.

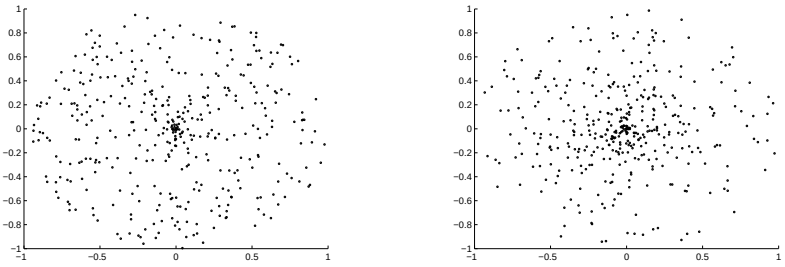

(a) (b)

Figure 3.8: *(a) Spray with* $f(\rho) = \frac{\log(1+\rho)}{\log(2)}$. *(b) Spray with* $f(\rho) = \frac{\sinh(\rho)}{\sinh(1)}$.

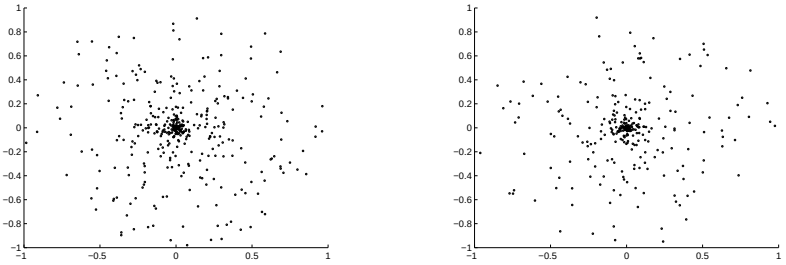

(a) (b)

Figure 3.9: *(a) Spray with $f(\rho) = \rho^2$. (b) Spray with $f(\rho) = \rho^4$.*

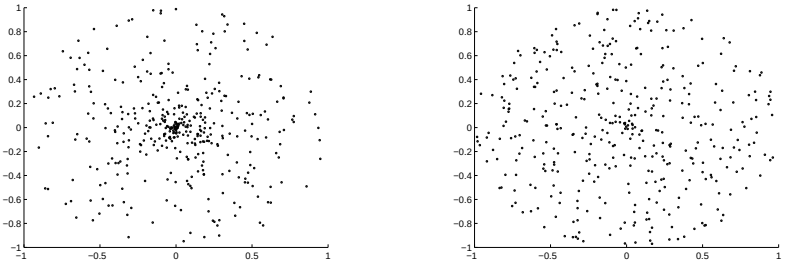

(a) (b)

Figure 3.10: *(a) Spray with $f(\rho) = \frac{e^{\rho}-1}{e-1}$. (b) Spray with $f(\rho) = \frac{e^{-\rho}-1}{e^{-1}-1}$.*

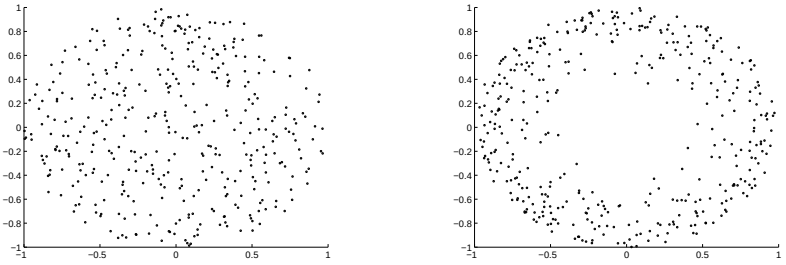

(a) (b)

Figure 3.11: *(a) Spray with $f(\rho) = \sqrt{\rho}$. (b) Spray with $f(\rho) = \sqrt[5]{\rho}$.*

RSR parameters and their meaning

RSR depends on four parameters: R (the radius of the sprays), f (the radial density function) N (the number of sprays) and n (the number of pixels per spray).

The radius R of the spray defines the extension of the circular area analyzed around the pixel i. This area must be tuned to get enough information about the color distri-

bution around i.

As already stated, the function f changes the radial density of the spray pixels. It must be tuned to find out what is the spray pixel distribution that better fits the computational reproduction of color perception performed by the HVS.

For each $Spray_k(i)$ there is a non zero probability to find the pixel with highest intensity x_{H_k} in an isolated pixel not related to the context. This, of course, would produce chromatic noise in the filtered image. Since the spray pixels are generated by a random point generator, all the N sprays are different and so, statistically speaking, the influence of isolated pixels on the global computation of $L(i)$ decreases when we average many sprays contributions $L_k(i)$. Hence, the higher is the number of sprays, the lower is the chromatic noise in the filtered image. This is confirmed by the tests performed (as will be discussed later), which also shown that, to avoid pattern replication all across the image, the sprays must be taken by a pre-computed set of, at least, a thousand sprays.

Finally, the number n of pixels per spray determines how much information is extracted from the spray area. If we use very large values of n we cover all the spray area, losing the locality of the spray distribution, instead, if we use small values of n, we cannot get enough information to correctly compute $L(i)$.

3.5.3 Tuning RSR parameters

We performed our tests on a set of over 100 very different pictures given by real-world images, portraits, landscapes and geometric images.

Tuning the spray radius

The easiest parameter to tune has proved to be the radius: for all images and independently from the other parameter of RSR, our tests showed that the optimal value for R is DIAG, the value of the diagonal of the image.

The reason is easily comprehensible: if one uses a smaller radius, then two pixels that lie near the extreme points of the diagonals can never be compared. The effect

of using a smaller radius than DIAG can be clearly seen comparing figs. 3.12 and 3.13, which have been filtered with $R = \text{DIAG}/2$ and $R = \text{DIAG}$, respectively, keeping all the other parameters constant: ρ as radial coordinate, $N = 30$, $n = 800$.

Figure 3.12: *An image filtered with spray radius* $R = \frac{\text{DIAG}}{2}$.

Figure 3.13: *The same image as in fig. 3.12 filtered with spray radius* $R = \text{DIAG}$.

Furthermore, it is not useful to use a radius larger than DIAG, since the spray loses part of its density around the target pixel and many spray points lie outside the image area.

Tuning the radial density function

The radial density of the spray is responsible for the local property of RSR because the probability to find out the pixel with highest intensity in the spray is greater in the image areas where the spray is denser, than in the image regions where the spray has only few points.

It is well known that tests about human color perception show that the chromatic influence between two pixels decreases with their distance (e.g.[24,23,50,134]). This fact is implemented in every color perception model: path-wise algorithms (e.g.[68]) sample the image content with paths that are denser in the immediate neighborhood of the target pixel than far away, while integrative algorithms (e.g.[54]) use a center/surround technique that weights the surround of the target pixel with monotonically decreasing functions.

Coherently with this, even RSR revealed that delocalized sprays are inadequate to correctly simulate color perception by the HVS. For example, fig. 3.14(b) shows the result of filtering the image in fig. 3.14(a) using $\sqrt[5]{\rho}$ as radial coordinate.

(a) (b)

Figure 3.14: *(a) Original "Gallery" image. (b) Effects of a spray with radial coordinate* $\sqrt[5]{\rho}$.

As a consequence, the only interesting radial density functions are those that correspond to monotonically decreasing radial densities. Only such functions will be considered in the next discussion.

We conducted the tuning using both subjective quality match tests and quantitative tests about color constancy.

The first kind of tests has been developed as follows: we filtered our test set of images fixing n and N and varying the radial density function. We have displayed the images on a middle gray background of a calibrated monitor in a dark room. Then we asked a collection of users to indicate in a scale between 1 (poor) and 5 (excellent), the

degree of naturalness (color plausibility in relation to the personal experience), absence of noise and detail visibility of the filtered images. The results of our tests, averaged on the three questions and on the test set images, are shown in Fig. 3.15.

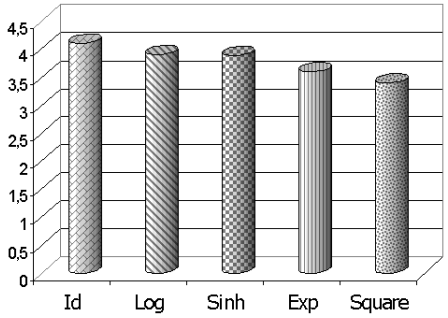

Figure 3.15: *Quality test for different radial density functions.*

The images filtered with the naturally localized spray have always received the best judgement by the users. Starting from ρ^2, the sprays results too localized and the corresponding filtered images show an increasing amount of noise, as can be seen in Fig. 3.16, that has been filtered with ρ^4 as radial coordinate and with $N = 30$, $n = 800$ (to be compared with Fig. 3.13, which has been filtered with the same values of n and N, but with ρ as radial coordinate).

Regarding color constancy tests, we considered the pictures of the database described in[98], consisting in a series of photographs taken under different color casts. We filtered each series of pictures with different radial density functions. Then we computed the CIELab differences between the images filtered with every given radial density function to have a measure of the corresponding algorithm ability to reduce color cast. This

Figure 3.16: *Noise induced by a spray with radial coordinate ρ^4.*

methodology is motivated by the fact that RSR always preserves the image content and does not collapses the dynamic range.

For more readability we report only the results of our tests on the picture in Fig. 3.17 taken under three different casts: Cast 1 = PHILIPS Neon Neutral Daylight 6500K (TLD965), Cast 2 = PHILIPS Neon Fluotone 4100K (TLD840), Cast 3 = PHILIPS Neon Daylight 5000K (TLD950). Tests with the others casts shown analogous results. We choose the database in[98] since it has been devised to test color correction algorithms without facilitating any of them. In fact, instead of choosing a white, gray or black background, we used two white noise backgrounds.

Figure 3.17: *An image of the database in[98] for color constancy tests.*

The values visualized in the graphics of Fig. 3.18 correspond to the parameters $N = 20$ and $n = 400$, when these parameters are varied the numerical values of the differences change, but the relationship between the different radial density functions does not change.

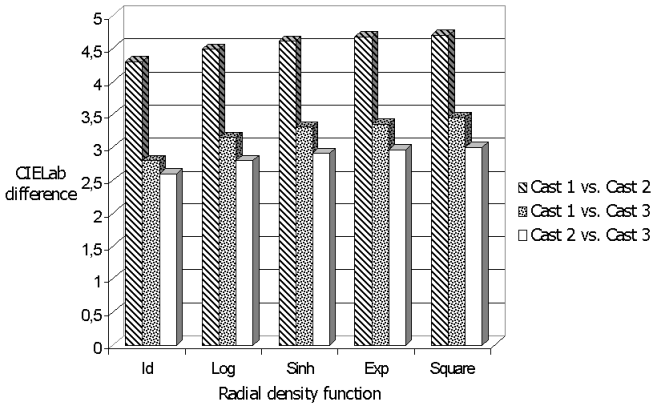

Figure 3.18: *Color constancy test for different radial density functions.*

It can be seen that the density function that minimizes the CIELab difference between the filtered images is the identity function. Tests on the other images exhibit analogous results.

The consequence of our subjective and quantitative tests is that the naturally localized spray is the most suitable to reproduce the behavior of the HVS within the RSR implementation of the Retinex model. From now on, RSR will be considered only with ρ as radial coordinate.

We recall from formula (3.12) that the areolar density of the naturally localized spray decreases as the inverse distance from the center. It follows that, in RSR, fixed a pixel i, every other pixel of the image, considered as a single entity, has a "mean chromatic influences" on i that decreases as the inverse distance from i. This fact implies that, statistically speaking, the chromatic influence of pixels close to i is comparable only with that of entire areas of pixels far from i, the wideness of which must increase, according to formula (3.12). This seems to be a good motivation to study multilevel extensions of RSR.

Finally, we notice that the result of this section corresponds to what found in the tuning experiments of another color perception model: ACE (Automatic Color Equalization)[97]. In that algorithm the target pixel is compared with the other image pixels, each of which is weighted with a coefficient. In[97] it has been shown that the optimal weight coefficients are the inverse distances from the target.

Tuning the number of sprays and pixels per spray

One of the consequences of the mathematical analysis performed in[89] is that, as the path length of a path-wise Retinex implementation grows to great values, the algorithm loses its local properties showing a global white patch behavior. The tuning of paths length or number is still an open problem for path-wise Retinex implementations.

We are now going to show that, with the RSR implementation, it is possible to perform an unsupervised tuning of the parameters N and n in a self-consistent way, highly reducing the range of their optimal values.

These two parameters are strictly related because the lightness is computed averaging the N contributions of the sprays, each of which depends on how many points are used to find out the pixel with highest intensity.

We carried out the tuning as follows. We filtered the images of our test set increasing N from 5 to 60 with a constant step of 5 sprays and increasing n from 250 to 900 with a constant step of 50 points. Then we calculated $\Delta E_N(n)$ and $\Delta E_n(N)$, the CIELab differences between the images filtered with a fixed value of N and two consecutive values of n, and viceversa, with N playing the role of n. We observed that both $\Delta E_N(n)$ and $\Delta E_n(N)$ decrease monotonically for all images.

Now, since two images are considered chromatically indistinguishable if $\Delta E < 1$, it is natural to tune N and n taking the smallest values of these parameters for which this inequality holds true. In other words, this procedure is a natural compromise between the minimization of filtering time and the maximization of filtering quality.

To have a quantitative example to discuss, let us consider the tests performed on the image in Fig. 3.19.

The interpolation graph of ΔE, viewed as function of N and n, and its intersection with the hyperplane $\Delta E \equiv 1$, is visualized in Fig. 3.20.

Fig. 3.21 and Fig. 3.22 represent the interpolation graphics of the functions $\Delta E_N(n)$ and $\Delta E_n(N)$, which are the level curves of the surface in Fig. 3.20. In the horizontal axis are indicated the two consecutive values of n or N corresponding to the CIELab difference values displayed in the graphic. Only the significant part of the curves are

Figure 3.19: *Image for the tuning of the parameters n and N.*

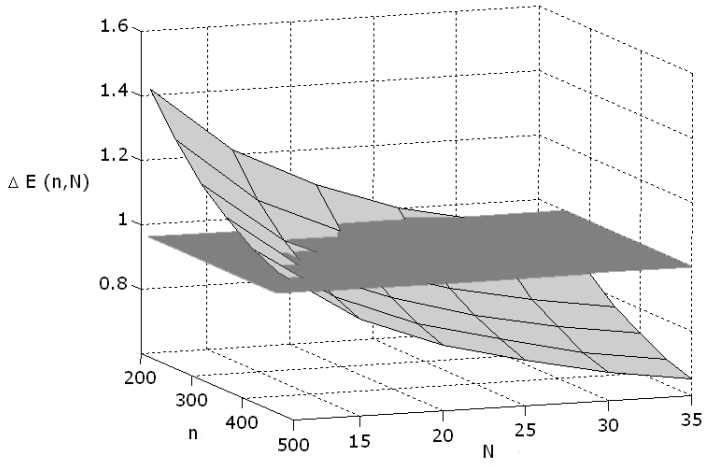

Figure 3.20: *Surface of $\Delta E(n, N)$ intersecting the hyperplane $\Delta E \equiv 1$.*

visualized.

Since the parameters n and N control two different characteristics of the filtered image, it is not sensed to take high values of n and little values of N or viceversa, because the corresponding image would have good chromatic quality, but high chromatic noise, or viceversa, respectively. Instead the optimal couple (N, n) must be chosen as the "minimal" couple of intermediate values of N and n such that the surface $\Delta E(n, N)$ lies under the hyperplane $\Delta E \equiv 1$, where with "minimal" we mean the couple that minimizes the product $n \cdot N$. For example, it can be seen from Figs. 3.21 and 3.22 that both the

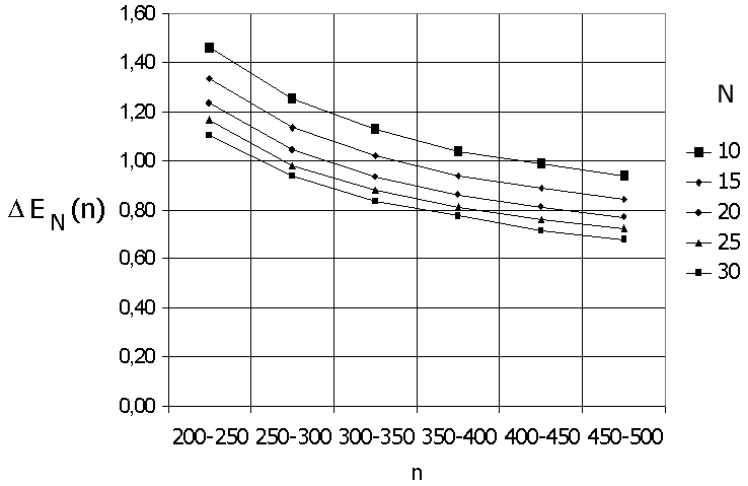

Figure 3.21: *Graphics of $\Delta E_N(n)$ for different values of N.*

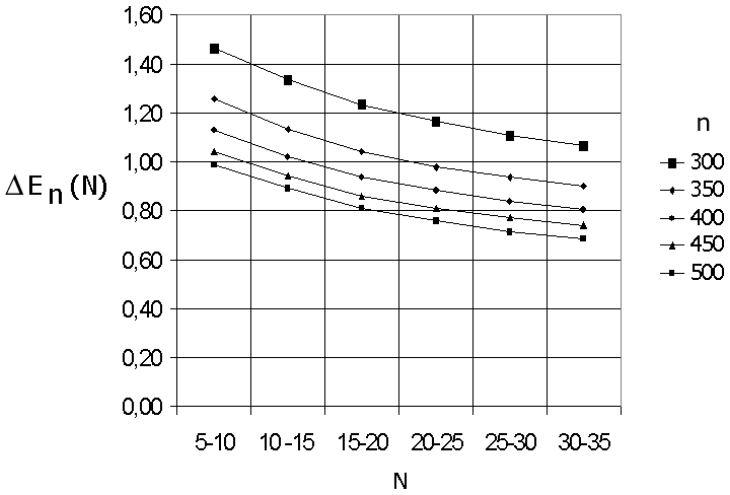

Figure 3.22: *Graphics of $\Delta E_n(N)$ for different values of n.*

couples $(N = 25, n = 350)$ and $(N = 20, n = 400)$ correspond to intermediate values of N and n such that the surface lies under $\Delta E \equiv 1$, but $25 \cdot 350 = 8750 > 20 \cdot 400 = 8000$, so that the optimal choice is $(N = 20, n = 400)$, because it corresponds to 750 operations per pixels less than the other couple.

We combined the procedure just described with subjective matches analogous to those performed for the tuning of the radial density function, but now changing every time the values of N and n. The results of the tests performed on the image shown in Fig. 3.19 are presented in Fig. 3.23. The surface is obtained interpolating the values at the nodes (n, N), the value at each node is calculated averaging the degree of naturalness, absence of noise and detail visibility indicated by the users.

It can be seen from the graphic in Fig. 3.23 that the surface reveals a wide constant area after the couple of parameters (N, n) overcomes $(20, 400)$, as predicted by the quantitative procedure described above. It is evident that there is no reason to increment the filtering time taking greater values for N and n. All the other tests performed has revealed agreement between the unsupervised procedure described above and the subjective tests involving users.

Now that we described the tuning procedure, we show in Figs. 3.24-3.26 some output results of RSR with tuned parameters (all the images in this section are courtesy of P. Greenspun).

As can be seen from the different values of optimal values of N and n for the various images, the tuning of N and n strongly depends on the different image content. The problem to find out a formula to precisely determine the variation of the parameters N and n in relation with the image content still remains open.

Filtering the same image with different sizes

If we consider a given image at different sizes, then we need a formula to extend the optimal values of N and n for a certain size to the other sizes of the same image. Our tests shown that the optimal value of N remains constant, but, as expected, the optimal value of n changes. In fact n determines the amount of information needed to compute the lightness and obviously this amount must increase or decrease in relation with the image size.

We can formalize the problem in this way: suppose we have the same image at the sizes $W_0 \times H_0$ and $W_1 \times H_1$, and suppose that $n^{opt}(W_0, H_0)$, the optimal value of n for the image of width W_0 and height H_0, is known. The easiest way to find out $n^{opt}(W_1, H_1)$, the optimal value of n for the image of width W_1 and height H_1, is to impose this mathematical proportion:

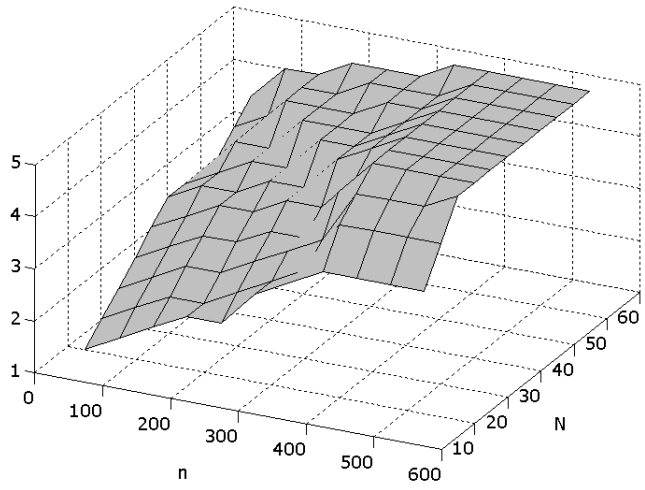

Figure 3.23: *Quality test for the parameters n and N with respect to Fig. 3.19.*

Figure 3.24: *"Gallery" filtered with tuned parameters:* $N = 25$, $n = 800$.

(a) (b)

Figure 3.25: *(a) Original "Books" image; (b) "Books" filtered with tuned parameter* $N = 25$, $n = 750$.

$$n^{opt}(W_1, H_1) : W_1 H_1 = n^{opt}(W_0, H_0) : W_0 H_0 \tag{3.14}$$

i.e to impose the fraction of spray pixels per unit of image area to remain constant.

Applying the unsupervised tuning procedure previously described, all the images of our test set shown that, once the optimal value of n is found for a given image size, formula (3.14) enables to correctly compute the changes of the optimal value of n in function of the new image sizes.

3.5.4 Future works on RSR

In the previous subsections we have described the RSR implementation and the tuning of its parameters. Obviously, many aspects need further analysis and consideration, so

(a) (b)

Figure 3.26: *(a) Original "flowers" image; (b) "Flowers" filtered with tuned parameter* $N = 20$, $n = 450$.

to contribute to the enhancement of the proposed computational model.

As suggested in subsection 3.5.3, future works will address surely the implementation of multilevel version and the problem to determine the variation of the parameters N and n in relation with the image content.

Moreover, the intrinsic parallel nature of Retinex algorithms (each pixel computation is completely independent from the others) make RSR very adaptable for parallel or distributed computation. Also the implementation of RSR as a fragment shader using some high level languages for GPU programming will be considered.

Finally, a merge between RSR and ACE[97] computational models is under consideration, so to develop an advanced algorithm that considers both color constancy than lightness constancy in an efficient way.

3.6 Comparison between Retinex algorithms: an open problem

In section 3.5 we have used the information resumed in section 3.4 to prove that if the path-wise structure is abandoned and it is substituted with the random spray structure, interesting information about local Retinex properties arises naturally[89]. This is, of course, a first step toward the *full* comprehension of the spatial properties of the Retinex model.

Naturally, there is a big interest in the comparison among spatial properties of the great amount of different Retinex implementations available in literature. However, we believe that this is a very challenging task and it should be considered still an open problem. The main reason is that local properties of a perceptual based color correction algorithm affect many features of its output images: contrast, frequency content, ability to remove color cast, saturation, pleasantness and quality. The perceptual analysis of these features shows that a proper perceptual comparison should face many difficulties, probably the most important is that there is not yet a universally accepted perceptual measure to compare image pleasantness, quality or contrast, hence such a comparison would be subjective. For an introduction on standard psycophysical measures (like e.g. panel tests, paired comparison, category judgment) see[29].

Moreover, differently from machine (or perfect) color constancy, the human color constancy property is far from being perfect and it depends on several factors such as temporal transients or illusive visual configurations.

Another great difficulty for a complete comparison is the fact that every Retinex implementation highly depends on its own parameters, whose tuning, in the few cases in which it has been performed[18], is based on very different criteria and image test sets.

Finally, by a theoretical point of view, a mathematical description of all the algorithms considered would be needed to create the basis for a common background where performing rigorous comparisons about the intrinsic properties of each implementation. Unfortunately, there still remain further Retinex implementations with no mathematical

characterization.

All the open problems briefly described above make a proper and exhaustive comparison an important yet difficult task that we deem interesting for future researches.

Chapter 4

Color in context and Tone Mapping

Contents

High Dynamic Range Imaging (HDRI) has become one of the most relevant research field of the last years: it has influenced the design and implementation of advanced acquisition devices, of new compression techniques for image and video formats, of advanced global illumination algorithms, of computational models of visual perception and of advanced display devices.

However, currently display devices supporting the direct visualization of HDR values are not still available, so there is the need to have mapping techniques that convert the large dynamic of the acquired scene to the supported values of standard output devices: the process that address this problem is known as *tone mapping*.

The complexity of this problem is particularly evident trying to display a HDR image of a scene with, for example, direct sunlight together with deep shadows: the remarkable adaptation mechanisms of the HVS make us perceive details in both areas when observing the real scene, where the application of simple numerical mapping techniques like a linear or logarithmic scaling will produce an output image too dark or too bright.

Many computational models (called *tone mapping operators* (TMOs)) have been proposed in the last years[93], each addressing the tone mapping problem differently. Since the HVS is too complex to be modelled completely, the proposed operators try to simulate only some particular perception mechanisms, like e.g. contrast sensitivity, color sensitivity and threshold versus intensity functions, using data from perceptual researches and experiments.

However, McNamara[75] noticed that HVS data considered so far derive from experimental set-ups that cannot test all the complex adaptive mechanisms active in natural scenes perception, on which usually a TMO should work. Following this idea, we decided to consider more the overall HVS behavior under natural conditions rather than some psychophysical data, derived from laboratory controlled conditions (so called "void conditions"). This approach is largely accepted by researchers in the *visual appearance* research field[64,107].

From our point of view, as researchers in color reproduction in imaging and computer

graphics field, the relevance of HDR images is obviously represented by the opportunity to consider as input tristimulus values commensurate to those physically measurable in a real scene, and consequentely to implement advanced color computational models that work in a more "realistic" context.

In this chapter we don't want to address in details all the basical aspects of HDRI and tone mapping, due to the great amount of scientific papers addressing these arguments. Moreover, a comprehensive book has been published recently[93], covering all of the aspects of HDRI cited at the beginning of this chapter.

We will just recall some relevant points, focusing more our attention on the problem of a correct color computation in the tone mapping field: to this aim we will present a Retinex implementation for the visualization of HDR images, called *HDR Retinex*.

4.1 Overview of TMOs state of the art

So far, several tone mapping methods have been developed. In the following subsections we will give only a brief description of some of the most representative TMOs proposed in the years. In section 4.2 we will comment in more details *if* and *how* color computation is addressed in TMOs state of the art.

Following the classification proposed in[93], four groups can be identified:

- *Spatial invariant* operators
- *Spatial variant* operators
- *Frequency based* operators
- *Gradient domain* operators

However, some of the spatial operators proposed present both invariant and variant mechanisms. In literature there is not an accepted convention about their classification: it is possible that in this dissertation some of the cited operators are classified differently than in other documents.

4.1.1 Spatial invariant operators

Spatial invariant operators apply the same global mapping function to all the pixels of the input HDR image: this is in contrast with all the evidences about the local behavior of HVS perception mechanisms. However, they are obviously characterized by a high computational efficiency.

The non-linear operator proposed by Tumblin and Rushmeier in 1993[122] is designed to replicate the variations in brightness as the illumination level in the scene change. This operator was later improved[121], and applied in an interactive algorithm based on the simulation of foveal adaptation.

In 1994, Ward[128] described a method that uses a linear scale factor to simulate contrast perception and visibility thresholds around a particular adaptation level.

In 1996, Ferwerda et al.[35] introduced a similar operator to match visibility threshold, but accounted for visual acuity and color sensitivity in relation to changes of the illumination levels.

In 2003, Drago et al.[27] introduced an operator based on logarithmic mapping. The logarithmic bases are adaptively adjusted according to each pixel's value, in order to preserve details and contrast.

In 2005, Reinhard and Devlin[91] proposed a dynamic range reduction algorithm inspired by photoreceptor physiology. This method presents an interesting tunable behavior able to achieve Von Kries-style color correction.

4.1.2 Spatial variant operators

Spatial variant operators change the mapping function according to the spatial context of the scene, therefore two pixels with the same value in the original image can be mapped to different values in the output image.

The operator described by Chiu et al. in 1993[14] scales the luminance value of every pixel using the average value computed on a neighbor set.

In 1995, Schlick[103] proposed a first degree rational polynomial function to perform

the mapping function. He applied it as a spatially invariant method at first, considering then three alternative techniques (low pass filtering, micro-zones and segmentation) for local adaptation simulation.

In 1997, Ward et al.[129], extending previous works, introduced a complex operator, that, starting from an analysis of the luminance histogram, computes the local adaptation levels used in the mapping process. The algorithm has been extended to simulate other HVS properties including visual acuity, color sensitivity and glare.

In 1997, Jobson et al.[54] proposed the application of their Multiscale Retinex on HDR images. Their algorithm is based on the original center/surround formulation by Land[65].

In 1998, Pattanaik et al.[88] described a complex multi-scale operator that simulates adaptation and spatial vision. The algorithm works by constructing a DoG pyramid from the original image, and applying to each frequency filtered image different gain-control factors, aiming at simulating the inner mechanisms of the HVS.

The LCIS operator proposed by Tumblin et al. in 1999[123] is based on a hierarchical decomposition of the input image in many sub-levels, each generated by solving a partial differential equation based on anisotropic diffusion.

In 2003 Johnson and Fairchild[55] applied the iCAM color appearance model[31] to render HDR images for display. The iCAM model consists in a chromatic adaptation step (based on Von Kries transform) followed by an exponential function. Like most color appearance models, the inverse application of the model is needed to prepare the image for display.

In 2004, Funt et al.[38] discussed the use of the implementation of the original Land's Retinex[66]. They followed the suggestion in[20] to avoid haloing problems. However they used the algorithm only on luminance without performing any color correction.

In 2002, Reinhard et al.[92] proposed a photographic tone reproduction method based on a two stage process: a first spatial invariant operator based on Ansel Adams' zone system and a second local operator based on center/surround contrast enhancement. A GPU implementation of this method has been proposed by Goodnight et al.[44] in 2003.

In the same year Kang et al.[57] applied a modified version of the photographic operator to convert HDR video.

In 2002, Ashikhmin[2] presented a three stage approach: the first stage estimates local luminance adaptation at each point of the image, the second stage applies a compression function on the input dynamic to the required display range, the last stage re-introduces details to the image by a local analysis of input local contrast.

In 2004, Rizzi et al.[99] proposed a modified version of ACE[97] algorithm (see subsection 3.3.3) for tone mapping. In the modified operator two non-linear controls have been introduced: the first control allows the model to find a good trade off between visibility and color distribution modifying the local operator at each pixel-to-pixel comparison, while the second modifies the interaction between pixels estimating the local contrast.

In 2005 Krawczyk et al.[61] proposed a framework for GPU real-time processing of HDR video that, starting from the application of Reinhard et al.'s photographic tone reproduction method[92], considers also visual acuity, glare, night and day vision.

In 2006, Krawczyk et al.[60,62] proposed a tone mapping operator inspired by an anchoring theory of lightness perception[42]. The method is based on the decomposition of an HDR image into areas (frameworks) of consistent luminance and on the local calculation of the lightness values. The final lightness of an image is calculated merging the frameworks proportionally to their strength.

4.1.3 Frequency based operators

Tone mapping may be achivied by transforming the original HDR data into a different representation: frequency based operators reduce the dynamic range of image components selectively, based on their spatial frequency.

In 2002, Durand and Dorsey[28] presented a one stage local non-linear operator in the framework of bilateral filtering. It uses two influence functions, one with arguments in the spatial domain, the other in the intensity domain.

In 2003 Choudhury and Tumblin[15] presented an operator based on trilateral filtering. The difference with bilateral filtering lies in the technique used to separate the image

into layers.

4.1.4 Gradient domain operators

Gradient domain operators search for large gradients in the input HDR data: these gradients are then manipulated before to compress the original dynamic range.

In 2002, Fattal et al.[33] presented a method that attenuates large gradients and then constructs a low dynamic range image by solving a Poisson equation on the modified gradient field.

4.2 TMOs and Color Computation

All the algorithms described in the previous subsections approach the tone mapping problem focusing only on some particular perception mechanisms. However, it is clearly evident how in nearly fifteen years of research in the implementation of TMOs, color perception mechanisms and their simulation have been rarely addressed, despite the undeniable relevance of these aspects in an attempt to simulate the experience of real observation of a scene.

Most of the operators usually derive a luminance channel from the HDR chromatic triplet in input, apply the compression of the dynamic range only to this achromatic channel, and then recombine the resulting values with the uncompressed RGB values to form the final tone mapped color image.

Looking at the few operators that explicitely consider color correction, we can distinguish between two different approaches:

- *Retinex-based approach*: the operators belonging to this group often apply in tone mapping field former Retinex implementations adjusted and accurately tuned for a correct computation of HDR values. Two examples of Retinex-based tone mapping operators are Jobson et al.'s Multiscale Retinex[54] and Rizzi et al.'s ACE algorithm[99]. Even the TMO operator proposed in this dissertation in the next section belong to this group.

- *Von Kries-based approach*: the other operators (Pattanaik et al.'s Multiscale Observer Model[88], Johnson and Fairchild's iCAM color appearance model[55] and Reinhard and Devlin's Photoreceptor Model[91]) solve color computation by following Von Kries hypothesis[125]. In its original formulation, this theory assumes that the brightest value found in each chromatic channel of the input image represent the reference white for that channel, and thus all the values are globally scaled consequentely.

It is a generally accepted fact that there does not exist a TMO that works perfectly for all images. Regarding color computation TMOs, some critical aspects are well-known:

- Retinex-based algorithms often suffer, as most of the spatial variant operators, for the presence of halos and artifacts, due to the local computation in areas characterized by high contrast gradients. Some efforts have been made to avoid these problems, adding local and automatic tuning of the parameters according to the image content[40].

- Von Kries-based algorithms must consider that one of the major flaws of the original Von Kries hypothesis to color constancy is its spatial invariant behavior: in critical cases the method is cheated by even a single highlight or noisy pixel.

4.3 HDR Retinex

In this section we propose a Retinex implementation for the visualization of HDR images. The operator, called *HDR Retinex*, is mainly based on the Brownian Retinex algorithm[69] described in subsection 3.3.1; however, we have improved the computational model, implementing a new methodology in the exploration of the input image, roughly inspired from the characteristics of eye movements, in order to tune the intrinsic color correction behavior of Retinex algorithms for a correct tone mapping of HDR images.

The new approach in the construction of the random paths have been mainly ideated and tested to tune the Retinex implementation to work with HDR data avoiding as possible halos and artifacts typical of local operators.

Regarding the observation process, we recall that it is composed by a sequence of two different stages: the movement of the eye, called *saccade*, shifting the gaze direction from a point to another, and a short interval between two saccades, called *fixation*. Information on the scene observed is taken only during fixations; no information is acquired during saccades[26,51,59,132,135].

4.3.1 Some comments about eye movements

The saccades movements are mainly due to the high concentration of cones (and thus to the high visual acuity) in the 2-5 degrees area of the retina, centered in the gaze direction, called fovea. Therefore human eyes must move to compensate the drop in both resolution and color sensing in the most part of retina outside the fovea.

However, the analysis of eye movements is a complex topic, due to the fact that saccades present both conscious and unconscious aspects[94].

Saccades are often affected by several elements, e.g. the context of the scene observed[135] (the eye moves in different ways if we are looking to a panorama instead of a room or a face, because different is the kind of information and features that must be analyzed).

Saccades could also be generated by a sudden visual stimulus, like a rapid light impulse or a moving feature in the scene, or they could be guided by specific intentions or decisions of the viewer[26], as the research in the scene of a particular object or the reading of a text; in some cases, even the past experience and the attitude of the viewer influences the eye movements[135].

Relevant are also the effects of memory and recognition: the second time we look at a room our eyes move differently compared to the first time.

A terminology has been proposed to address the different processes of visual attention mechanisms, that rule the movements of the eye during the observation of a scene: this

terminology distiguishes between *bottom-up* and *top-down* processes[6]. *Bottom-up* processes are automatic and unconscious mechanisms, that are supposed to be ruled by the presence of some features in the scene attracting the attention automatically. *Top-down* processes are, on the contrary, task-dependent mechanisms, i.e ruled by predetermined intentions of the observer (e.g searching for an object).

In the perceptually-based rendering field, many computational models have been proposed to automatically determine *regions of interest* in an input image, so to set the best rendering quality only where the attention of the viewer is predicted to be most attracted.

Models that try to simulate *bottom-up* processes extract features from an image that are presumed to attract the attention of the viewer: *saliency maps*[58,52,34] are constructed analyzing edges, orientations, high frequency regions, intensities etc.

On the other hand, models simulating *top-down* processes are based on *task maps*[67,79,80] that highlight task-relevant objects in the input image.

Even if the results are promising and quite useful for many applications, they are not good enough to predict very accurately eye movements: the main problem is that real vision presents both of the *bottom-up* and *top-down* aspects at the same time, and these algorithms only address one of them at a time. Some works[71] have investigated the discrepancy between real eye movements captured using *eye tracking* devices and the results of the cited algorithms.

Some recent works[10,111] investigated how to use both *saliency maps* and *task maps* together to have a more accurate simulation.

A comprehensive description and validation of these methods can be found in[110,85].

4.3.2 Our approach

In this dissertation we have decided to not consider the techniques illustrated in the previous subsection.

Evidently, task-dependent approaches are not suitable for the purpose of this dissertation, but, on the other hand, it has been proved that *bottom-up* methods are not

sufficiently accurate[71] to simulate precisely eye movements. Probably this is due to the influence of some "personal" behaviors of the observers, as memory of the scene, recognition of some objects, sudden interest for particular features or details in the image, that "shift" in some way the unconscious and automatic observation (the "bottom level") up to some "higher level" of visual attention. It is evident that such particular aspects are very hard (if not impossible) to be simulated.

Therefore, even if a good approach to avoid artifacts and problems in spatial invariant tone mapping operators is to consider local image content to adaptively tune their parameters, as suggested in subsection 4.2, we have decided at the moment to ignore these issues. However in subsection 4.3.8 we will discuss about a more accurate consideration of eye movements in the implementation of the proposed computational model using *eye tracking* devices.

We have decided to modify the random paths construction procedure of the original Brownian Retinex implementation, with the aim to obtain paths that in an abstract way have some characteristics noticeable in real scanpaths of eye movements.

We can notice that many eye scanpaths[132] generally present an alternation between different types of saccades: quick jumps among largely spaced points and shorter shifts. Visually this alternation consists in a sequence of some segments that lie almost on the same line, that suddenly changes direction (see movements circled in fig. 4.1).

This is more evident where the eyes are not attracted to some specific points of attention (e.g. eyes and nose in fig. 4.1): in that cases the scanpaths appear more crumbled.

Ignoring all the complex components that have influence on voluntary saccades, whose computational simulation is still an open problem, we tried to construct random paths with both the characteristics described above (quick jumps and shorter shifts) in a uniform way across the image, and whose appearance resembles those that can be observed in many eye scanpaths, as the one circled in fig. 4.1.

We would like to recall that our approach does *not* intend to exactly simulate eye movements, but only to take inspiration from them in order to develop an efficient

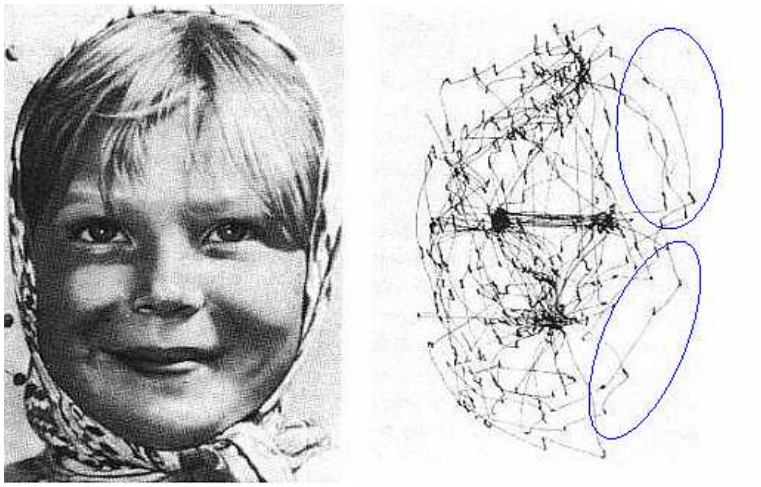

Figure 4.1: *An example of eye scanpath[132]: in the ovals the path structure we have tried to simulate.*

exploration of the image. To this aim, we have made some experiments focusing our attention on the random distribution of the mid-point displacement algorithm[102], that rules the position of the points of the paths in the image, and therefore their final shape.

As discussed in the next subsections, we applied uniform and Gaussian distributions in the recursive steps of the algorithm in order to obtain a sequence of different shifts in the paths. Moreover, we propose an alternative technique to compute Retinex ratios on the generated paths.

A preliminar description of the experiments have been published in[39].

4.3.3 The algorithm

To speed-up HDR Retinex computation, a set of 5000 paths have been calculated and saved on an external text file using MATLAB^{TM}.

During computation, for each pixel in the input image N paths are randomly selected from the set, and then Retinex ratio-reset mechanisms are applied on the pixels of each path. The resulting value for each path is added to the final contribution for the considered pixel. Finally, contributions are averaged, and the final results are linearly scaled to the available dynamic range of the ouput device and saved to file. In fig. 4.2

```
Load_HDR_Image( immin );
Load_Paths( paths );
for each row r {
     for each column c {
          Select_N_paths();
          for each path p {
               result = Apply_Ratio_Reset( r,c,p );
               Add_To_Chain( result );
          }
          Average_Contributions();
     }
 }
 Map_to_Output();
 Save_LDR_Image( immout);
```

Figure 4.2: *Pseudo-code of HDR Retinex algorithm*

pseudo-code is used to resume algorithm steps.

The only two parameters to set are the number N of paths to consider for each pixel, and the levels of recursion of the mid-point displacement algorithm, that rule the number of pixels condidered in each path. We have found that considering 250 paths per pixel and 2 levels of recursion (i.e. each paths is composed of 5 points) leads to good results for almost all the HDR images considered.

However, in fig. 4.3 and 4.4 we show as example paths composed by a different number of pixels: this is due only for a better explanation of the chosen techniques.

4.3.4 Testing different random distributions

Looking at the structure of the algorithm, in subsection 4.3.3, is evident that testing different random distributions in the paths construction process does not affect Retinex computation: simply, different external files containing the different kind of paths are

passed as input to the main program.

Applying Uniform distribution

We have initially considered only uniform distribution in the calculation of the random shifts, obtaining as results very crumbled paths, largely spaced across the image, with long jumps from one point to another, similar to the first saccades type cited in subsection 4.3.2. Examples of this kind of paths are graphically shown in fig. 4.3, marked with circles.

Using paths constructed only with uniform distribution in Retinex computation, we observed in output a good color recovery effect in all the situations, but with poor rendition in dark areas (see fig. 4.5(a) and 4.6(a)).

Applying Gaussian distribution

Trying to simulate the other saccades type cited in subsection 4.3.2, the shorter shifts, we needed a random distribution that gives as results little displacements for the middle points of the segments in the various levels of recursion of the paths construction algorithm.

Our choice was to use Gaussian distribution in the algorithm instead of the uniform, because the obtained Gaussian paths are almost straight, presenting much smaller shifts, exactly the effect of this kind of movement (see the paths marked with squares in fig. 4.3).

Using in the Retinex algorithm paths constructed only with Gaussian distribution we have obtained slightly brighter and more detailed images, but, in most cases, with halos and artefacts, due to both the Retinex reset mechanism and the strong Gaussian paths directionality (see fig. 4.5(b) and 4.6(b)).

Applying both distributions together

In the third experiment we have tried to simulate the two movements together. To this aim we used the uniform distribution only in the first level of recursion of the mid-point

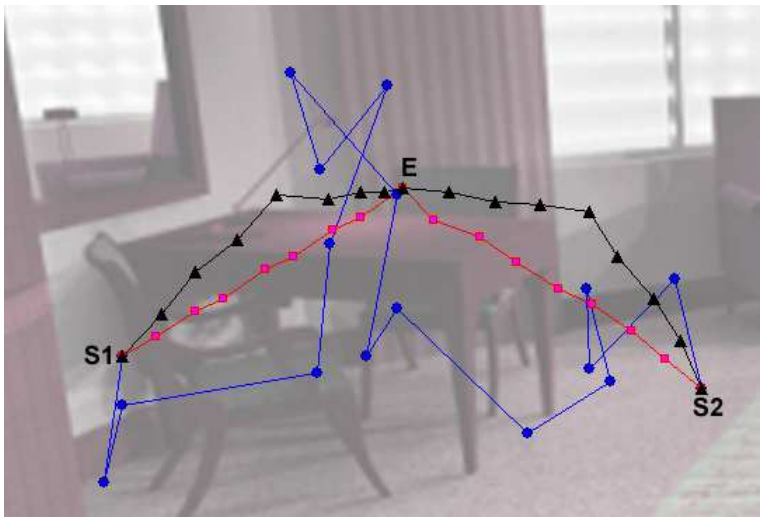

Figure 4.3: *An example of paths (from point S1 and S2 to point E), constructed applying uniform distribution (lines with circles), Gaussian distribution (lines with squares), and both distributions together (lines with triangles).*

displacement algorithm, and the Gaussian distribution in the other levels, generating paths with both the characteristics of the saccades types considered in subsection 4.3.2 (see the paths marked with triangles in fig. 4.3). These paths are quite similar to those indicated in fig. 4.1.

The images filtered using in the Retinex algorithm paths constructed using this new technique have the same brightness of those filtered using Gaussian paths, but with halos and artefacts removed in many images (as fig. 4.5(c)).

However, undesired artefacts are still present in some images (e.g. fig. 4.6(c)) in which bright light sources of reduced dimensions cause the presence of small areas with high local contrast that lead to a relevant reverse gradient effect.

4.3.5 Scanline vs Sampling

The results obtained with the experiments illustrated in subsection 4.3.4 are promising, but not completely satisfactory: the enhancement in the overall brightness of the output images obtained using both distributions must be improved.

Thus, we focused our attention on *how* the paths are used to compute Retinex ratios.

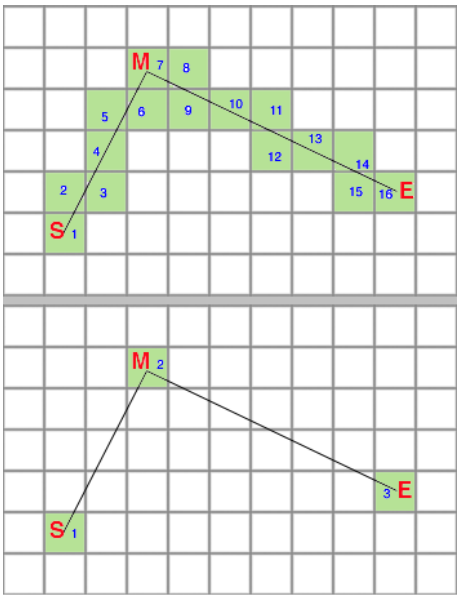

Figure 4.4: *Schemes of Bresenham algorithm (top) and of the proposed method (bottom). In the first case Retinex algorithm is applied on all the marked pixels, in the second case it is applied only on the line terminal points.*

In fact, the basic Brownian Retinex uses the Bresenham algorithm[7] to determine all the pixels along a path segment.

Retinex ratio-reset mechanisms are then applied on all the pixels involved by a path, as shown in the top half of fig. 4.4.

In the saccades analogy, this could be as considering the eye capturing information from all the points during its movement, but this is not what happens: information is acquired only during the fixations. Thus vision can be considered a kind of *sampling* process of the information of the observed scene.

Consequently, we decided to simulate this sampling process computing the Retinex ratios only on the terminal points of each segment chain (see bottom half of fig. 4.4), without scan converting each path segment.

The obtained results are satisfying: the images are pleasant and appear natural, with a relevant enhancement of their overall brightness. Also color recovery is enhanced, one example is the sky in fig. 4.5(d); it can be noticed that halos and artifacts still present in some previous results are now completely eliminated, like in fig. 4.6(d).

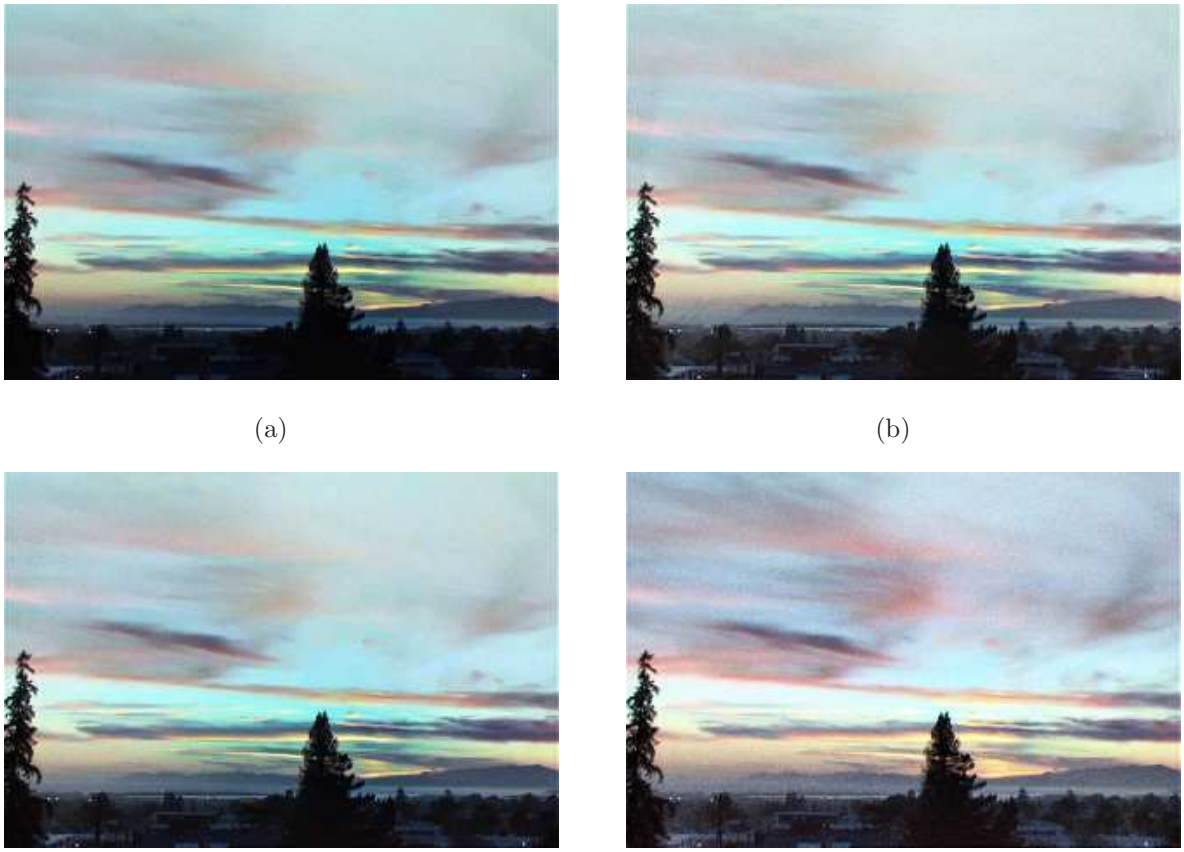

(a) (b)

(c) (d)

Figure 4.5: *Images filtered with paths constructed applying uniform distribution (a), Gaussian distribution (b) and both distributions together (c). Retinex ratios are applied to the pixels determined by the Bresenham algorithm. In fig. (d) the ratios are applied instead only to the terminal points of each path. See the evident artefacts near the street lamps in the bottom left corner of fig. (b), and how they are eliminated in fig. (c). Also, see the improvement in the color rendition of the sky and of the clouds between fig. (c) and (d). The images are no gamma corrected. Original HDR image by Paul Debevec.*

4.3.6 Discussion of the results

In fig. 4.9 to 4.16 some results of the computation of HDR Retinex are shown. All images have been filtered using 250 paths per pixel (each path composed by 5 points) constructed using both uniform and Gaussian distribution, and applying the sampling

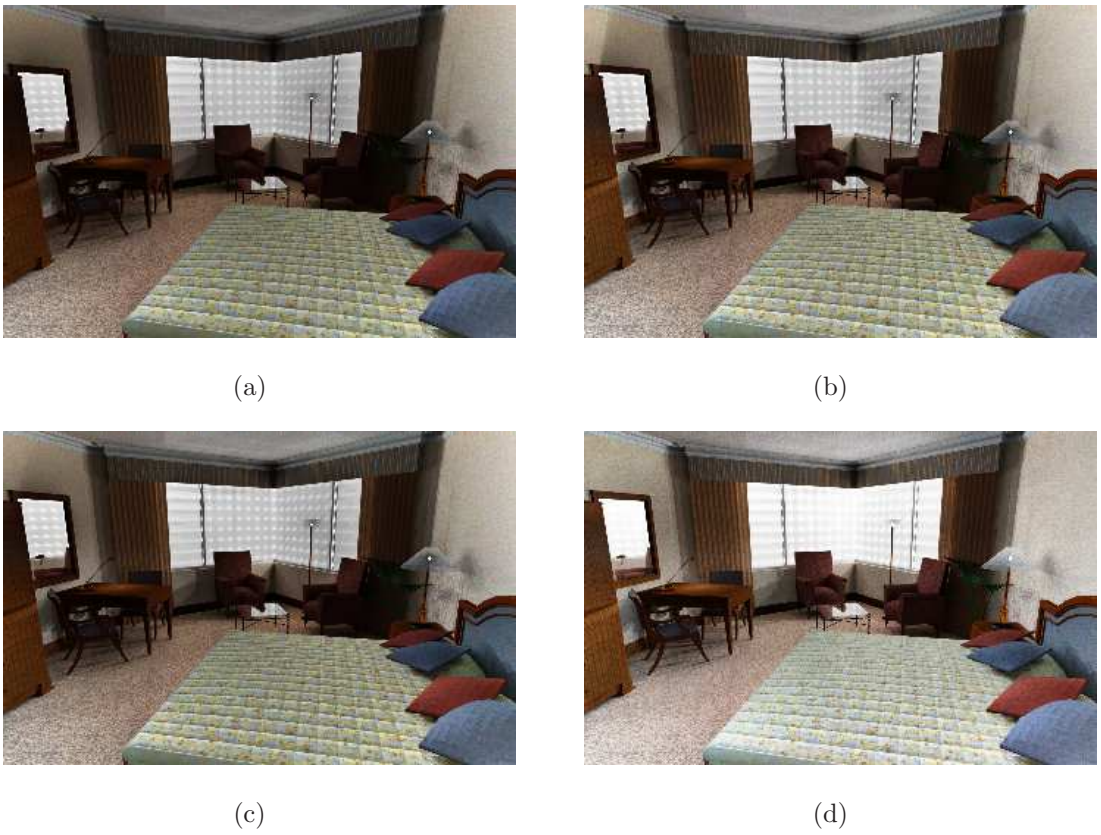

(a) (b)

(c) (d)

Figure 4.6: *Images filtered with paths constructed applying uniform distribution (a), Gaussian distribution (b) and both distributions together (c). Retinex ratios are applied to the pixels determined by the Bresenham algorithm. In fig. (d) the ratios are applied instead only to the terminal points of each path. See the evident halos in fig. (a) and the artefacts in fig. (b) around the light sources. In fig. (c) we notice only an attenuation of the undesidered features, still present and relevant. In fig. (d) artefacts are completely eliminated and the image brightness is improved. The images are no gamma corrected. Original HDR image by Simon Crone.*

technique to compute Retinex ratios.

HDR Retinex performs very well in a great number of situations; however, unfortunately is not yet a perfect computational model.

Some results are affected by gaussian noise: it is particularly evident on some old images of synthetic scenes, with poor details and textures, and on some of the older HDR images obtained applying Debevec and Malik's well-known algorithm[25]; in more recent

HDR images noise is completely absent or not noticeable. In particular the results of the application of our operator to HDR images acquired by last-generation CCDs able to capture directly all the dynamic range of a scene with a single pass[106] are completely noise-free (fig. 4.15 and 4.16). We will investigate if the presence of noise may be due to some errors in the calibration or interpolation of the input data to the Debevec and Malik's algorithm.

The obtained results show that our operator is able to avoid halos and artefacts in many situations where other spatial variant operators fail. Some problem still occurs in very extreme situations, where very large gradients still cause some gradient reverse effect. An example is shown in fig. 4.7. This is probably due to the fact that in this situation glare simulation must be considered, but this effect is not considered in original Retinex theory.

Some problems occurr also in extremely dark HDR images, characterized by *scotopic* viewing condition, because Retinex theory was introduced to explain color perception in *photopic* viewing condition only, when cones are completely stimulated.

4.3.7 Parallel implementation

Retinex algorithms are generally computationally expensive. To avoid this, often some speed-up techniques are applied, like e.g. multilevel approaches or LUT-based algorithms.

HDR Retinex computation has been optimized as much as possible: paths have been precomputed and saved to external file, logarithmic conversion is applied before the main "for" cycles, conditional statements have been avoided when possible. The sampling process introduced to compute Retinex ratios contributes also to obtain better performances. Unfortunately, computational time needed is still relevant.

However a good characteristic of HDR Retinex is its intrinsic *parallel* nature: a pixel computation is completely indipendent from its neighborood, and also the three chromatic channels are computed indipendently.

We have tested a parallel version of HDR Retinex on a HP 9300 XW workstation

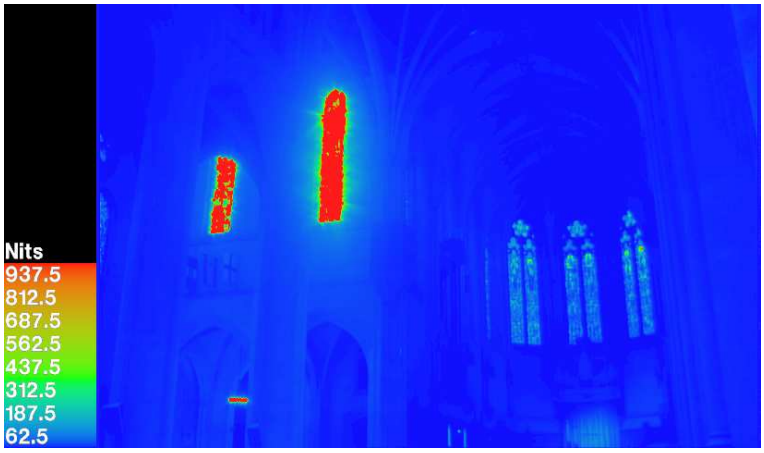

(a)

(b)

Figure 4.7: *One of the few images where HDR Retinex does not avoid halos: here is presented a false color image to show the very large gradient near the windows (a) and the obtained image after HDR Retinex computation (b). Even though the filtering of the windows is quite good, gaussian noise and halos are present in the neighborood. Original HDR image by Paul Debevec.*

with two AMD Opteron dual core at 2.0 GHz and 3 GB of RAM. To parallelize the code, we have just added simple OpenMP[84] preprocessor directives before the first "for" statement of fig. 4.2, without any other relevant changes in the original C code. Given R the number of rows of the input image, $R/4$ rows are assigned and indipendently

Dimensions of input image	1 Processor	4 Processors
256x256	13 s	3 s
512x512	63 s	15 s
1024x1024	272 s	65 s
2048x2048	1135 s	290 s

Table 4.1: *Performances of HDR Retinex on a single processor and on four processors (AMD Opteron at 2.0 GHz) using OpenMP*

processed by each of the 4 computational cores of the workstation.

We have investigated the computational performances between the original version (i.e. using a single processor) and the parallel implementation (using four processors), filtering HDR images at increasing resolutions. The results, shown in table 4.1, confirms, as expected, that parallel computation is 4 times faster.

These results are very promising, because a relevant diffusion and implementation of multi-processor architectures (like e.g. the CELL architecture[11]) is attended in the next years.

4.3.8 Future works

Regarding HDR Retinex implementation, we are investigating mechanisms to "weight" the contribution to the ratios of the pixels of the paths according to local properties of the input image, e.g. considering a measure of local contrast, in order to tune the computation when very large gradients occurr.

Moreover, there are some other aspects we will address, regarding speed-up methods and different computational environments.

Local Linear Lut (LLUT)

In 2006, Gatta et al.[41] proposed an algorithm called Local Linear LUT (LLUT) to speed-up the computation of high computational cost color correction algorithms, like

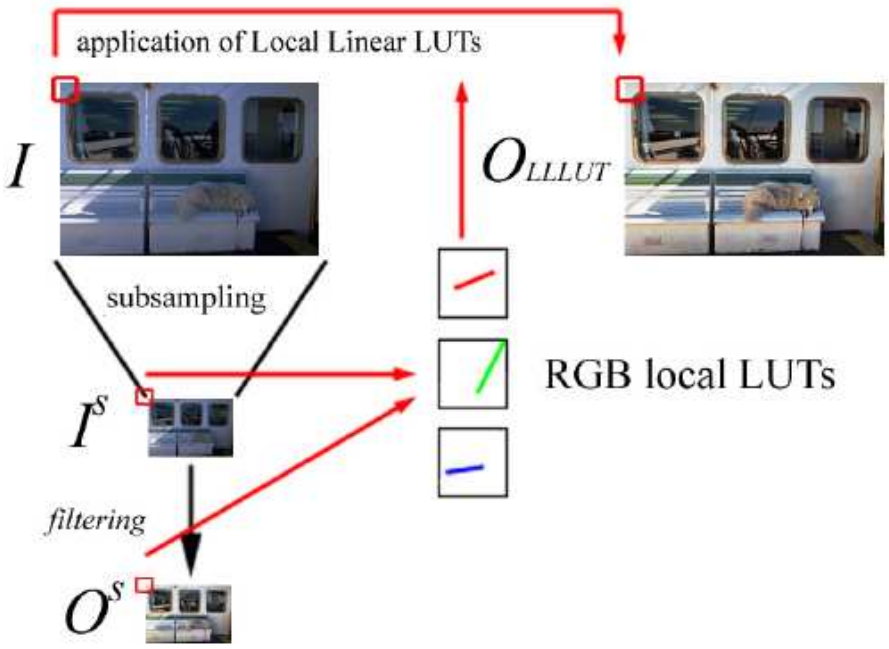

Figure 4.8: *Scheme of LLLUT algorithm.*

Brownian Retinex or ACE. The main idea of LLUT is to apply the color-enhancement algorithm only to a small sub-sampled version of the input image, and to determine a local linear interpolation function to apply to the image at the original resolution in order to maintain the local filtering effect. A scheme of the algorithm is shown in fig. 4.8.

LLLUT is a very appealing approach to consider together with the parallel implementation of HDR Retinex to achieve good computational performances, even for HDR video processing.

However, to overcome possible loss of detail due to sub-sampling, the authors introduced in LLUT implementation an optional and additional stage to maintain high-frequency content. Unfortunately, an accurate tuning of this stage (that, for Brownian Retinex, is quite similar to the last step of the Ashikhmin's TMO[2]) is still an open problem.

We think that probably best results may be achieved applying as interpolation method some kind of *non-linear* function based on the frequency content of the input

image, rather than reintroducing high frequency information as additional stage.

GPU implementation

The continuous growth in computational power of the graphics processors (GPUs) of today's video cards, and the availability of high level programming languages for graphics hardware has brought to a great interest on GPU programming in the computer science community.

Many researchers have exploited the highly parallel nature of GPU architecture "mapping" general purpose offline computations on graphics hardware originally designed for video games development. This research field is known as *"General Purpose computation on GPU (GPGPU)"*[46].

This is not a straightforward process, since the programming model and environment have some rigid constraints that do not allow just a trivial conversion of usual CPU applications: often the developers are forced to completely reimplement the structure of their algorithms. Moreover, only single precision arithmetic is available, and this could be a serious limit for some scientific calculations where high precision is absolutely necessary.

In subsection 4.3.7 we have discussed about the parallel nature of HDR Retinex: therefore the proposed computational model is well suited for SIMD pipelines of GPUs pixel processors.

We want to investigate the technical problems in implementing the algorithm on GPU, as using only single precision arithmetic, storing random paths set into textures in GPU memory, avoiding texture access overhead, considering instruction limits, implementing an efficient multipass approach using e.g. Frame Buffer Object extension to OpenGL.

Moreover, we want to compare the computational performances between the GPU implementation and the parallel multi-CPU version introduced in subsection 4.3.7.

Probably even the GPU implementation of HDR Retinex will need some speed-up technique to achieve real-time performances: we will implement a GPU version of

LLLUT to address this problem.

Towards Virtual Reality applications

Currently, different solutions for immersive visualization of Virtual Reality (VR) scenarios are available. High-end devices like CAVEs or 150° cylindrical screens allow to consider a more realistic simulation of the observation process, because viewing conditions are not limited to simply looking at a monitor: eyes and head movements are more similar to those noticeable during real observation of a scene.

Otherwise, obtaining real-time high quality visualization in VR environments is a complex goal, due to the very high resolution images to be processed and displayed to achieve the sensation of being *inside* the virtual world.

In subsection 4.3.1 we have discussed about eye movements, their nature and the computational solutions proposed for their simulation in the perceptually-based rendering field.

An interesting research in this field, proposed by Chalmers and Cater[12], show how the visual acuity and visual attention mechanisms can be considered to obtain real-time high quality rendering. The main idea, supported by some experiments involving many observers, is that outside foveal resolution low quality rendering can be considered: it has been proven that observers do not notice any difference.

We want to investigate a similar approach to implement a real-time Retinex-based TMO for VR environments, based on the relevation of eye movements using a *eye tracking* device, that computes a high level filtering only into the foveal area centered around gaze, and a fast, low-level filtering outside foveal resolution.

Figure 4.9: *Original HDR image by Paul Debevec.*

Figure 4.10: *Original HDR image by Paul Debevec.*

Figure 4.11: *Original HDR image by Greg Ward.*

Figure 4.12: *Original HDR image by Paul Debevec.*

Figure 4.13: *Original HDR image by Cornell Program of Computer Graphics.*

Figure 4.14: *Original HDR image by Fredo Durand.*

Figure 4.15: *Original HDR image by Spheron AG*[106].

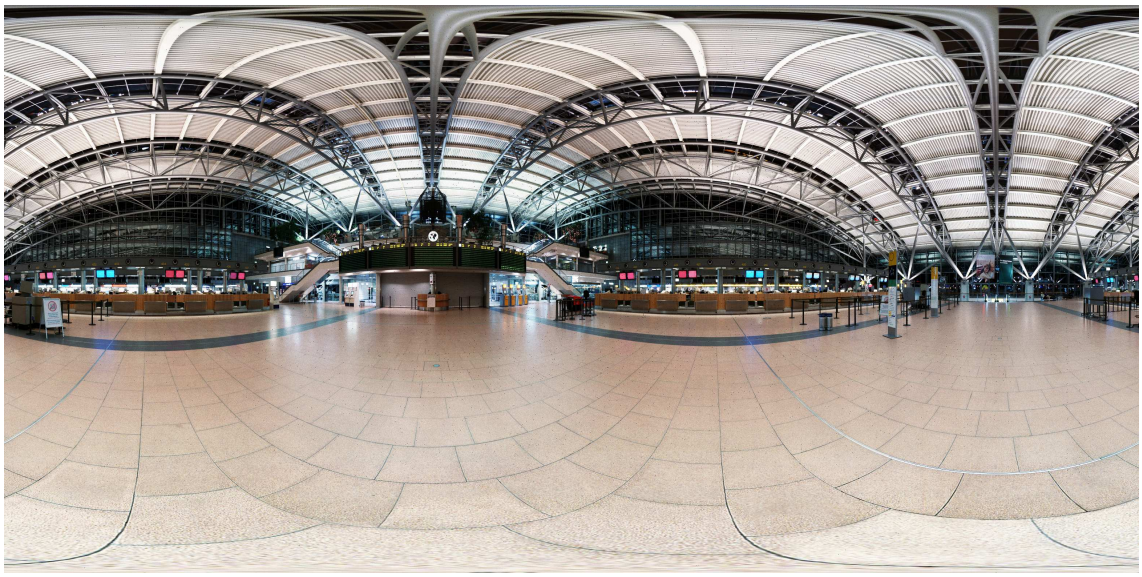

Figure 4.16: *Original HDR image by Spheron AG*[106].

Chapter 5

Spectral information and spatial color computation

Contents

The overall process of color sensation consists of two steps: the first is the *retinal* color stimulus generation, the second is the analysis of this color stimulus made by the HVS perception mechanisms. In the previous chapters we have addressed the explanation of these mechanisms, and their computational simulation in the imaging and computer graphics research field. We have stated the relevance of considering accurate computational models in order to achieve a correct and realistic color reproduction.

In this chapter we want to focus, in a computational way, on the relation between retinal color stimulus and the following perceptual processing, in order to investigate if spatial color computation is affected by changes in the determination of tristimulus values or if, otherwise, it is able to decrease the effect of changes in the triplet definition.

From a physical point of view, color stimulus comes from the interaction between spectral light distributions and surface reflectances: when this resulting spectral distribution comes to the eyes retina, three values per point are generated by the three different kind of cones (L-cones, M-cones and S-cones, so called because their sensitivity peaks are situated in long, medium and short wavelengths).

In colorimetry, a set of *Color Matching Functions (CMFs)*, or alternative integration curves are used instead of cone responses, in order to convert continuous or stepwise spectral information into a triplet of chromatic values.

CMFs are determined on the basis of *visual matching* experiments[131], and they have the role to supply a usable numerical definition of "color" applicable in many fields of science and technology. On the other hand, cone responses have been only estimated[109] and not directly measured, and their numerical range is not well-suited for pratical applications.

In the next sections we will give a brief historical overview about colorimetry researches and CMFs determination, and also we will introduce some comments and discussions about the former experiments and the data used to set the actual colorimetric standards, the so-called *Standard Observers*. We will then present an experiment to investigate how spatial color computation can decrease the effect of CMFs variation on

color rendition in synthetic image generation.

5.1 CIE Standard Observers

Even if many researches in the colorimetry field have been done in the last 75 years, only two standard observers have been currently proposed by the *Commission Internationale de l'Eclariage (CIE)*.

In 1931 CIE used the results from the experiments of Wright (1929) and Guild (1931) to determine the *2° CIE 1931 RGB Standard Observer*[16,131], graphically shown in fig. 5.4. Both the experiments have been done considering only foveal vision in controlled conditions, to avoid the *rod intrusion* effect, i.e. the stimulation of rods in the periphery of retina, that was considered to introduce distortions in the final results.

Following Grassman's laws[131], CIE decided to determine and apply linear transformations to the RGB curves in order to obtain a new set of curves, known as the *2° CIE 1931 XYZ Standard Observer*[16,131] ,with specific features: the most important requirements were that the new curves had non-negative values and that the Y curve must be equal to the photopic luminous efficiency function $V(\lambda)$[131]. To notice how Judd in 1951[56] and Vos in 1978[126] proposed modified versions of $V(\lambda)$ that better consider sensitivity at wavelengths below 460 *nm*; these results led obviously to changes in the determination of XYZ curves.

The XYZ Standard Observer is a more "abstract" color system, in the sense that the numerical triplet used to determine a color is not directly related to some mixture of spectral "basical" wavelenghts, as in RGB Standard Observer, but it expresses an acromatic stimulus plus two adimensional parameters.

In 1959 two different experiments have been done by Stiles and Burch[108] and Speranskaya[105] in order to consider also extra-foveal conditions. The relevant problems in considering a larger visual field (10° in both the experiments) have been related to the contribution of rods rensponse outside the fovea (the previously cited *rod intrusion* effect) and to the so-called *Maxwell spot* effect, i.e. the presence, in some cases, of an

irregular area centered in the gaze direction that appears non-uniform to an observer, even if the color stimulus presented fills uniformly a large field. This is due to the presence of a yellow pigment (called *macular pigment*) over the photoreceptors in the retina, whose concentration is greater close to the fovea and declines highly moving out into the peripherical areas.

The visual matching setups and conditions considered in the two experiments were quite different: Stiles and Burch removed explicitely the rod intrusion effect considering only photopic conditions in their tests, and asked the observers to simply ignore central area to eliminate the Maxwell spot effect, avoiding rods stimulation; Speranskaya does not address the rod intrusion at all, but instead she avoided Maxwell spot effect masking the 2° central area in the visual matching setup. However, the obtained results are quite similar, in fig. 5.4 are represented the curves determined by Stiles and Burch.

In 1964 CIE decided to establish the *10° CIE 1964 RGB Standard Observer* for large-field vision, starting from the results of these experiments: Judd[17,131], acting for the CIE, first of all applied numerical transformations to the Speranskaya results, to eliminate distortions due to rod intrusion, then averaged these new values with those from Stiles and Burch experiments; however in the merging process he gave more weight to the Stiles and Burch results.

Following the same approach of the 2° Standard Observer, linear trasformations have been applied to the new curves to determine the *10° CIE 1964 XYZ Standard Observer*[17,131].

5.2 Comments on CIE Standard Observers and other researches

Many scholars have proposed comments and discussions regarding many aspects of the former experiments and of the CIE standard determinations, also considering that in the last 75 years many new results regarding vision processes knowledge have been proposed, and also more advanced technologies are now available

to adopt in the visual matching experiments.

In the official CIE documents[16,17] on Standard Observers definition some mathematical details are missing regarding the merging procedures of the original data sets from Wright, Guild, Stiles and Burch, Speranskaya experiments, and also the description of the applied linear transformations for RGB to XYZ spaces conversions are incomplete. Researches regarding the reconstruction of these missing steps have been proposed only recently: in 2004 Broadbent[8] attempted to reproduce the steps taken in the definition of the 2° CIE 1931 Standard Observer, while similar works regarding the 10° CIE 1964 Standard Observer determination have been proposed by Trezona and Parkins[120] in 1998 with a further investigation by Trezona[119] in 2001.

In a series of six papers[112,113,114,115,118,116] published in 1992, Thornton, using multiple alternative primary sets and considering particular cases regardind strongly metamerical stimuli, presented results that appear to challenge Grassman's laws, that are the basical assumptions of the definition of CIE 1931 Standard Observers, and therefore he suggested that CIE standard curves are not the best choice for the characterization of a standard observer. In the articles he also described new setups and data for a more correct definition of color matching experiments and curves. The results presented by Thornton in his articles have been further analyzed and extended in 2004 by Oulton[86,87].

In 1997 Fairman et al.[32] analyzed in details the principles adopted by CIE in each step of the definition of the 2° CIE 1931 Standard Observer from the results of Wright and Guild experiments, in order to critically examine, after six decades of new researches and knowledge, if those first assumptions would be acceptable and adoptable reformulating from the beginning the definition of the Standard Observer, and their conclusion was that none of the original principles would be suitable today.

On the contrary, other scholars, like e.g. Fairchild in 1989[30] and North and Fairchild in 1993[82,83] defended the adequacy of the CIE 1931 Standard Observer.

More recently some efforts have been done in considering more natural vision conditions in the determination of new CMFs, starting from new scientific proposals stating that also peripherical areas of retina are involved in visual processes, and that the 10°

field considered in the CIE 1964 Standard Observer is not sufficient to simulate extra-foveal situations adeguately: this has led to *large field* color matching experiments[49].

5.3 Our approach to CMFs

In this dissertation we do not want to analyze the mathematical steps in the determination of the Standard Observers, nor to discuss details about experimental setups used in the colorimetry field, rather we are interested in investigating the effect of different choices of CMFs when color transformations is considered in the context of complex scenes.

In fact, in visual matching experiments CMFs have been proposed considering color as an isolated stimulus, in comparison with a control one, without considering all the perceptual mechanisms illustrated in the previous chapters of this dissertation that show how color sensation is highly contextual.

Another interesting point is that a recent research[48] prove that the spatial distribution of cones in human retina has high variance among different subjects: we would expect a corresponding difference in subjective color perception, that however has not been observed. This suggests that some perception mechanisms compensate this variability, as suggested by many studies on visual perception[1,136,66,9,125]. A second element that reinforce the existence of a compensation mechanism for spatial color perception is the evidence that human cones spectral sensitivities are highly overlapped and uneven[131,109], and moreover they are very different from proposed CMFs.

We ask therefore what is the relationship between contextual models of color perception and different CMFs: to this aim, computer graphics techniques are useful to simulate first steps of human vision and color generation, applying different sets of CMFs to synthetically generated spectral color distributions in order to calculate tristimulus values.

The question addressed in the next sections is to investigate how spatial color computation can decrease the effect of CMFs variation on color rendition in synthetic image

generation. To this aim we have devised an experimental setup to test the interdifference among tristimulus colors obtained using different CMFs and the change of this interdifference when a spatial color correction is applied.

In the next sections we will describe the experimental setup and we will present a discussion about the obtained results.

5.4 Description of the experimental setup

We have organized our approach to color rendition in a pipeline, shown graphically in fig. 5.1, where the ovals on the right represent the main stages of the experiment and the rectangles represent the inputs and outputs of each step. This pipeline is at the basis of our experiment.

In the first stage, a global illumination algorithm computes the interaction between spectral light distributions from light sources and surface reflectances of a synthetic scene. The renderer generates a high dynamic range spectral luminance distribution, due to the accurate photometric characterization of light sources specific of the software.

In the second stage, the multispectral image computed by the renderer is converted into a high dynamic range RGB image, applying three chosen CMFs. In fig. 5.2 false colors give a hint on the luminance values of the test scene used in our experiment.

In the third and last stage of the pipeline a tone mapping operator is applied to convert the high dynamic range to the available dynamic range of the output device (a monitor).

In this approach, the RGB values of the HDR image, output of the second stage, represent the *retinal* color stimuli from a "colorimetric" point of view, i.e. they are a simulation of the retinal response, while the chromatic triplets in the final LDR image represent the *perceived* colors, the output of the processing of the perception mechanisms of the HVS, computationally approximated by the TMO.

Obviously, if the chosen TMO does not address color computation, but only some kind of luminance mapping, then the resulting RGB triplets are strictly related to the

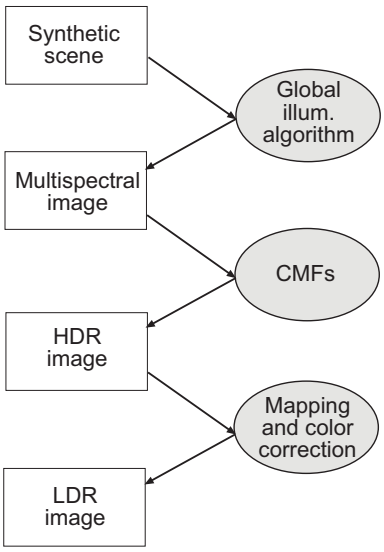

Figure 5.1: *Color rendition pipeline*

retinal color stimuli determined in the previous stage of the pipeline.

In our experiment, after the generation of several HDR images using different sets of CMFs, each representing a possible characterization of color sensitivities from a colorimetric point of view, we have applied to each HDR image three different TMOs, with and without color computation.

Our goal is to evaluate the effect of color computational models applied to different characterizations (due to different choices in CMFs) of retinal color stimuli, and to this aim we applied ΔE measures between LDR images obtained applying the same TMO on HDR images generated from different CMFs. In fig. 5.3 is shown the scheme of our experiment, whose details are described in the next subsections.

Our expectations are that when a TMO with no color computation is applied, the resulting distances will be relevant, because different values and characteristics of the integrating curves lead to an evident variability in the generated color stimuli, while we expect a remarkable reduction of the ΔE values when color computational models are used, justifying the hypothesis that perceptual mechanisms exists that compensate the interpersonal variability of cone responses and therefore subjective difference in retinal color stimuli generation.

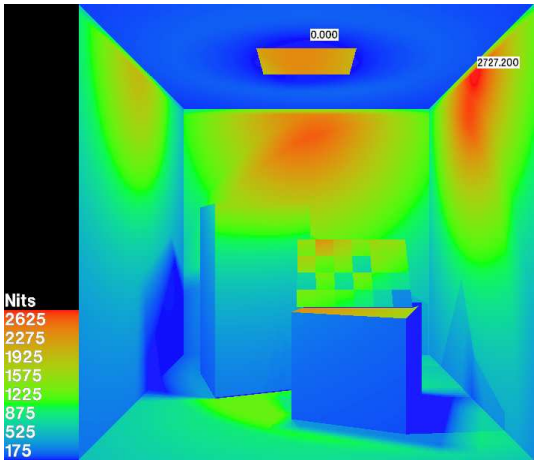

Figure 5.2: *False color image of the synthetic test scene. Luminance values range from about 0 to 2700 cd/m2 for D65 configuration.*

5.4.1 Multispectral image generation

First of all we have built a synthetic scene, similar to the Cornell box[45,21], containing a simplified Macbeth-like color checker. The Macbeth-like color checker has been characterized by the same reflectances as the original one, without the patch gray separation, to simplify its geometrical description.

We have then generated two multispectral images using a photometric raytracer by Rossi et al[101], that samples, for each pixel, spectral luminance in 80 frequency values ranging from 380 to 775 nm at increments of 5 nm.

The two multispectral images have different illuminants configuration: the first has two D65 light sources, while the second has one A and one C illuminant. In both cases the positions of the sources are the same: the first in the center of the ceiling, the second in the top left corner, pointing to the opposite corner.

In the following sections we call these two configurations *D65 configuration* and *A/C configuration*.

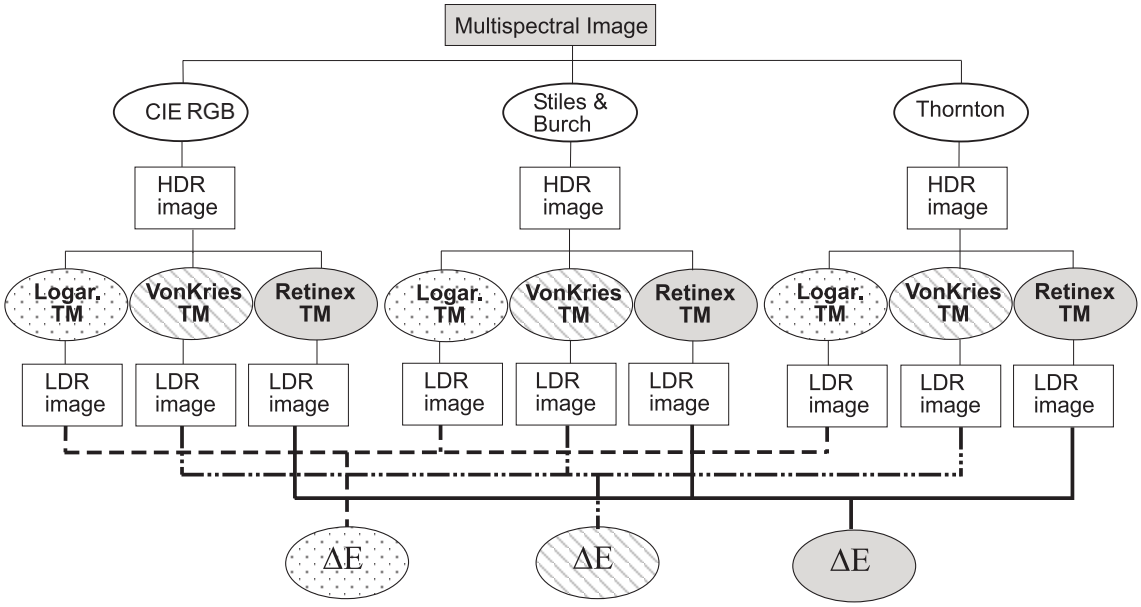

Figure 5.3: *Scheme of the experiment for each illuminants configuration.*

5.4.2 The chosen CMFs

In our experiment we have chosen three sets of CMFs, defined by established researches, with different characteristics. The chosen curves differ about experimental setups and technologies, and have different peaks wavelength and values, and different numerical ranges.

Applying curves with different peaks wavelenghts and corrispondent heights values to the multispectral image give us very different retinal stimuli (i.e. HDR images) and therefore a good test to analyze the effect of the application of color correction models. In 1999 Thornton[117] demonstrated how the choice of the peaks wavelengths in color matching experiments has effect on the peaks values in the resulting curves.

We have tested:

- CIE 1931 RGB curves[16,131], because they are the most used standard for RGB conversion.
- The set of CMFs proposed by Stiles and Burch[108,131], because they contribute to the standard 10° CIE 1964.

- A set of curves that Thornton gave us by personal communication, because they are a recent example in the direction of CMFs improvement.

The shape of the three sets of CMFs is graphically shown in fig. 5.4.

5.4.3 The chosen TMOs

In the proposed pipeline, TMOs are introduced to mimic in some way some HVS perception mechanisms in order to transform the retinal stimuli in input (represented by the HDR image) into the perceived signals, stored in the output LDR image. From a computational point of view, there is also the need to map the large dynamic range of the HDR image into the supported range of the output devices, as explained in chapter 4.

We have seen in section 4.2 that the few proposed TMOs that address color computation follow Retinex[66] (see chapter 3) or Von Kries[125] theory, while the other algorithms adopt some kind of luminance mapping.

We have decided to consider all these approaches, and therefore the chosen TMOs adopted in our experiment are:

- A simple logarithmic mapping method that, like a generic gamma correction, *does not perform any color adjustment.*
- A basical Von Kries algorithm, that implements a *global spatial color correction.*
- The HDR Retinex algorithm described in section 4.3, that implements a *local and global color correction.*

We therefore have at the end a set of LDR images representing nine simulations (three for each illuminant configuration) of perceived color signals (see fig. 5.3).

We have decided to use two generic and simple algorithms rather than consider other published and well-known methods because currently we are interested in the overall approach of the processing methods, i.e the presence or not of color correction

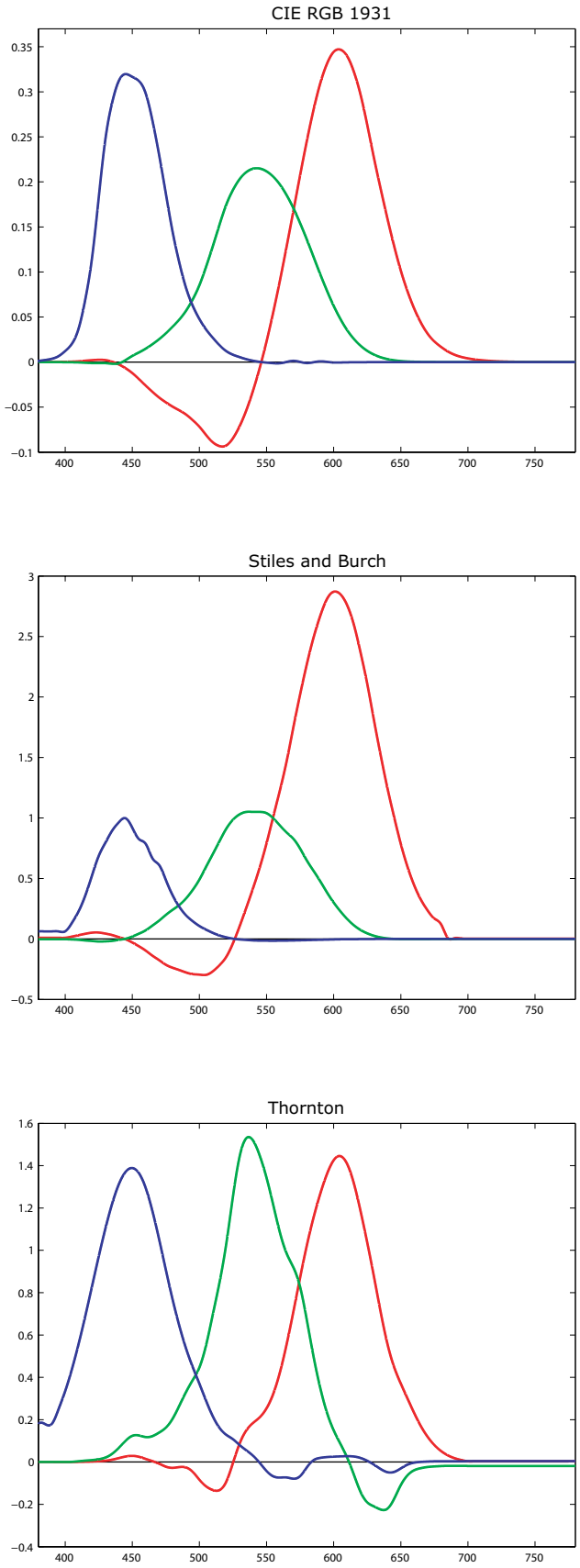

Figure 5.4: *Graphical plot of the considered CMFs.*

mechanisms, and eventually if color computation is implemented in a global or local way.

In this dissertation we have discussed about how color perception have a contextual nature, about how color computation is essential in our opinion in imaging and computer graphics applications and about the strong local characteristics that a good computational model must have.

On this basis, we want to show in our experiment first of all that not considering color computation in a TMO leads to a serious lack in the simulation of perception mechanisms: therefore we have decided to consider a general algorithm as a representative of an entire family of computational models.

We have decided also to not consider at the moment other TMOs that implement global color computation, because an exaustive analysis of their inner structure is needed in order to not present unfair comparisons, and this is over the objectives of this dissertation: in some algorithm color correction is not the main characteristic, but a secondary option, when in other methods the computation is ruled by a set of parameters to set manually. Again, we have chosen a general TMO that present a simple global color computation to represent the entire category, leaving a detailed comparison between all the color correction TMOs published in literature as a future research.

5.4.4 Discussion of the results

To evaluate how much the choice of CMFs affects the color rendition in the image synthesis pipeline, we have applied euclidean ΔE measures in perceptually uniform CIELab space between LDR images obtained applying the same TMO (see fig. 5.3).

To better investigate the relations between different spectrum information and color computation we present an average of ΔE measures computed on the single patches of the virtual Macbeth color checker between a couple of images. We have considered a neighbourhood around the patches centers excluding the edges.

Some interesting conclusions arise from the analysis of the results, shown in fig. 5.7 for D65 configuration and in fig. 5.8 for A/C configuration.

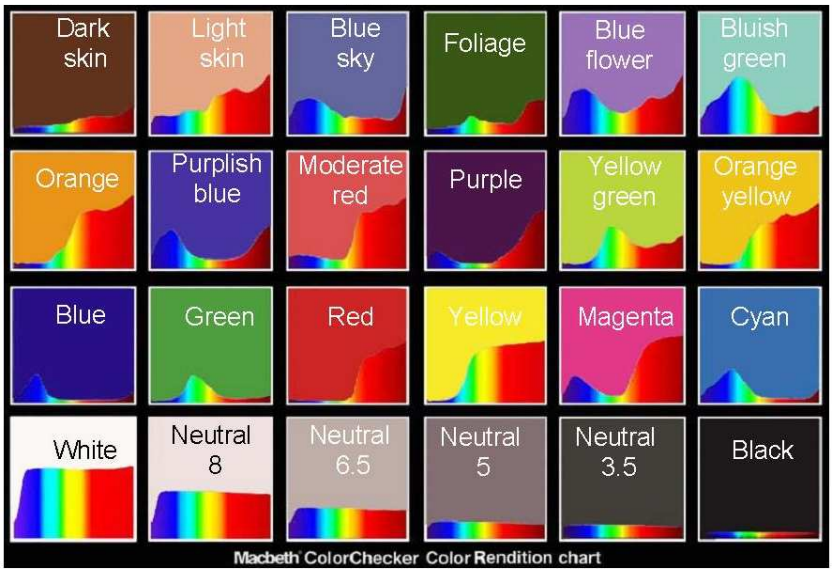

Figure 5.5: *Spectral characterization of the MacBeth color checker patches.*

First of all, it is evident that the logarithmic mapping, without color computation, exhibits a considerably higher interdifference with respect to the two color in context correction methods. Moreover, Retinex TMO shows an overall more stable behavior at changes in retinal stimuli generation.

We can also notice a relation between the spectral characterization of the patches (see fig. 5.5) and the obtained results: ΔE measures suggest a stronger attenuation effect obtained by contextual color computation in grey patches and in some low saturation colors (like e.g. Yellow Green patch), while in the patches on the third row (Blue, Green, Red, Yellow, Magenta, Cyan), where the role of peaks wavelenghts and heights is more relevant, the distance values are higher, even if the effect of color correction models still is very impressive.

Moreover, excluding the less significative (from a numerical point of view) values, in the results regarding the patches of the third row we can find cases where Von Kries global color computation seems to perform better than HDR Retinex color correction.

These effects are more evident in the A/C configuration results (fig. 5.8) where a strong reddish dominant is introduced by the A illuminant, leading to a chromatic shift in the generated tristimulus values.

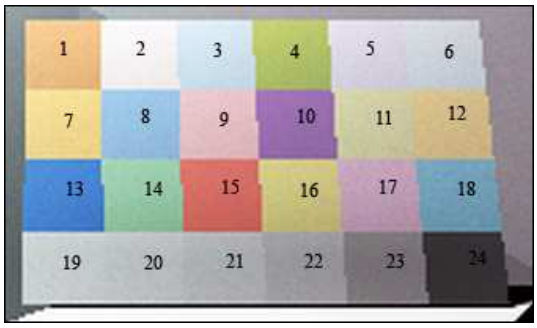

Figure 5.6: *Numerical legenda for images 5.7 and 5.8.*

The results seem to confirm our initial hypothesis that subjective differences in retinal color stimuli generation are compensated by the HVS color perception mechanisms.

However, the values regarding the patches on the third row suggest that a deeper investigation about peaks wavelengths and heights in CMFs determination is needed, and therefore that colorimetric researches in that sense still play a relevant role. In 1999 Thornton in a previously cited paper[117] demonstrated how the peaks wavelengths in most of the CMFs determined in color matching experiments fall near the same wavelenghts (near 450, 540 and 600 nm), but that moving even slightly from these primaries lead to a relevant increase in obtained peaks heights.

Two interesting details in the numerical results are that for black patch in fig. 5.8, for Stiles and Burch vs. Thornton CMFs, ΔE measure is 0 for HDR Retinex color correction method, while in fig. 5.7, for CIE rgb vs. Styles and Burch CMFs, we can find in the Light Skin patch the only case where the logarithmic mapping results in a lower interdifference than Von Kries global color correction method, but still Retinex shows a lower interdifference.

The figures 5.9 and 5.10 display the computed images in D65 and A/C configuration. It is evident from a visual comparison that higher degree of color normalization is the result of a contextual color correction. In fact fig. 5.9(a) shows clearly a high interdifference, which is much less noticeable in figures 5.9(b) and 5.9(c). In A/C configuration we observe the same behavior.

The presented results have been published in[96].

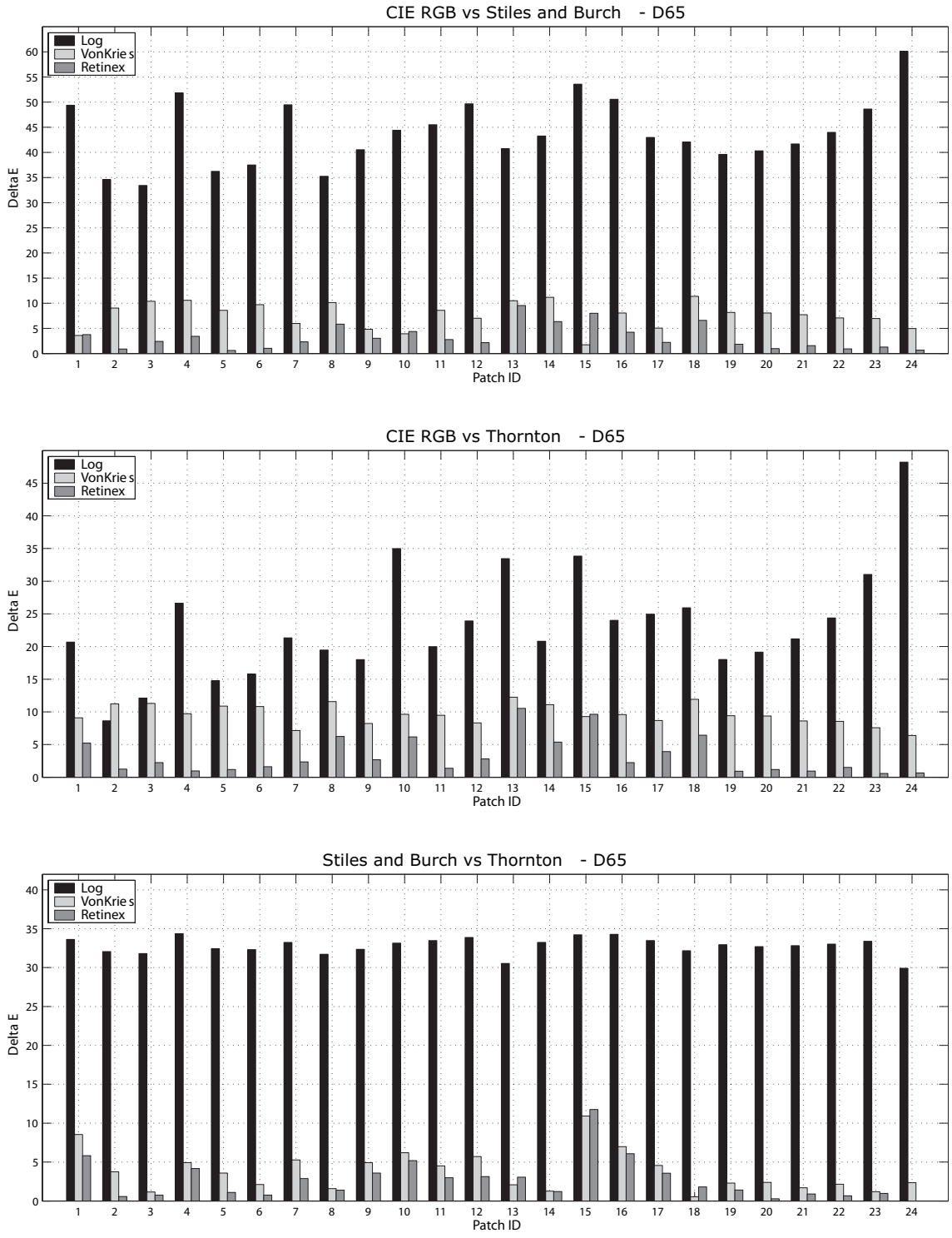

Figure 5.7: *Average ΔE on each patch. Numbers on x axis correspond to patches, as in 5.6. Three diagrams are for D65 illuminant.*

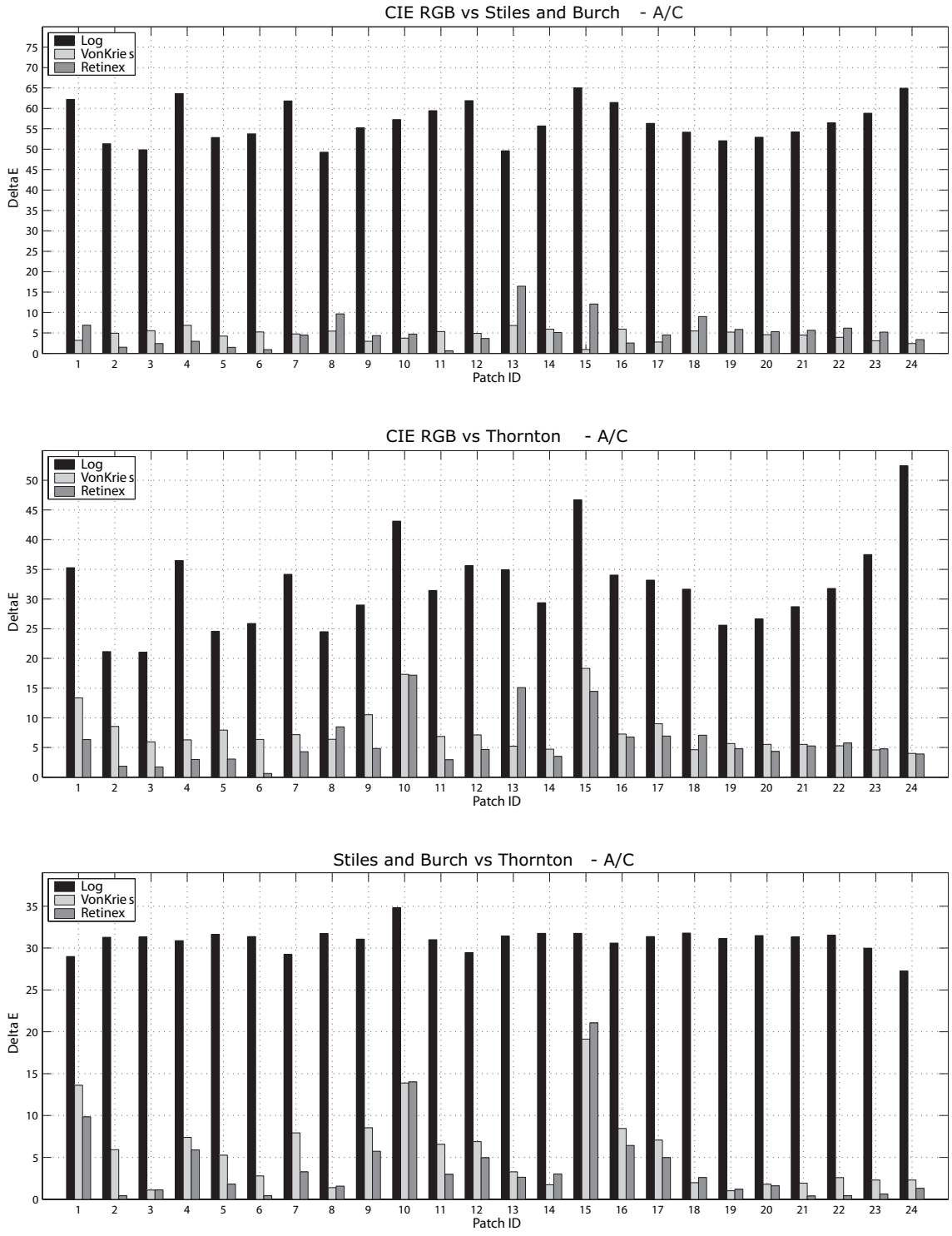

Figure 5.8: *Average ΔE on each patch. Numbers on x axis correspond to patches, as in 5.6. Three diagrams are for A/C illuminant.*

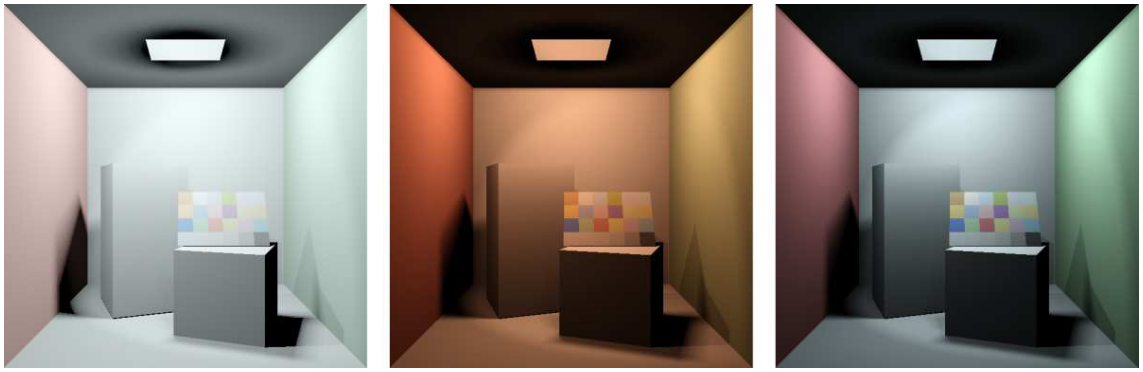

(a) Logarithmic mapping

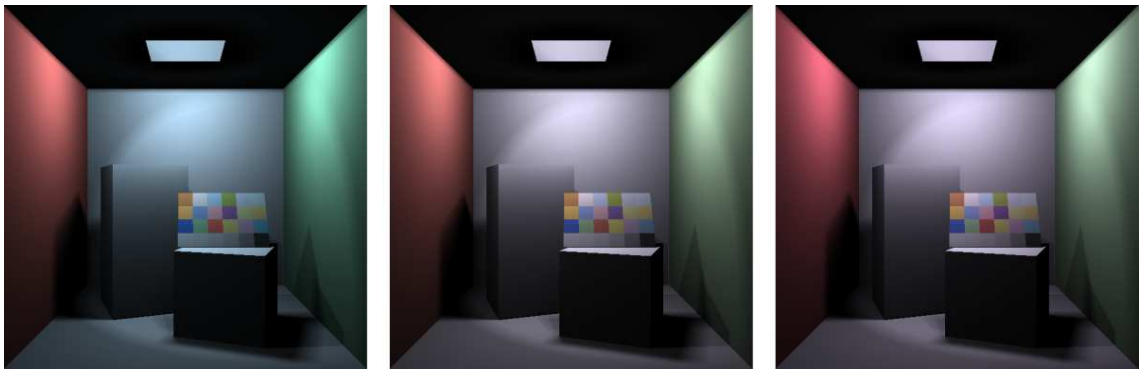

(b) Von Kries color correction

(c) Retinex color correction

Figure 5.9: *D65 illuminant. CIE RGB (left), Stiles and Burch (center) and Thornton (right) CMFs.*

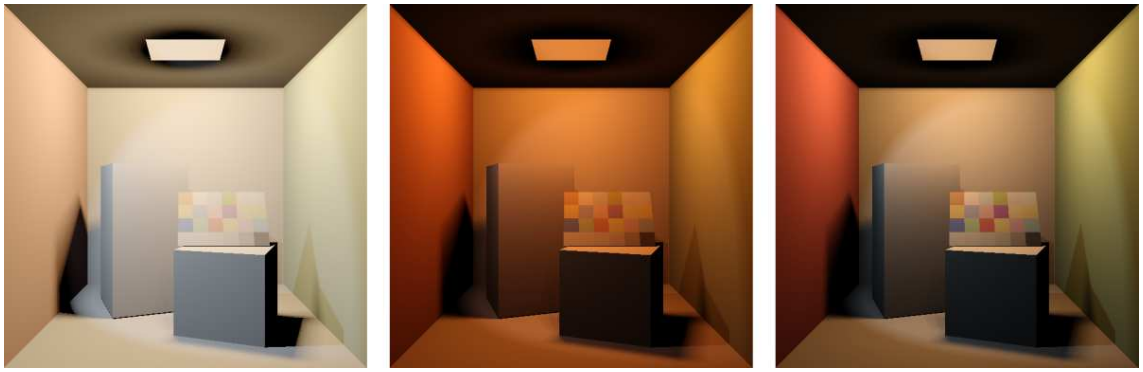

(a) Logarithmic mapping

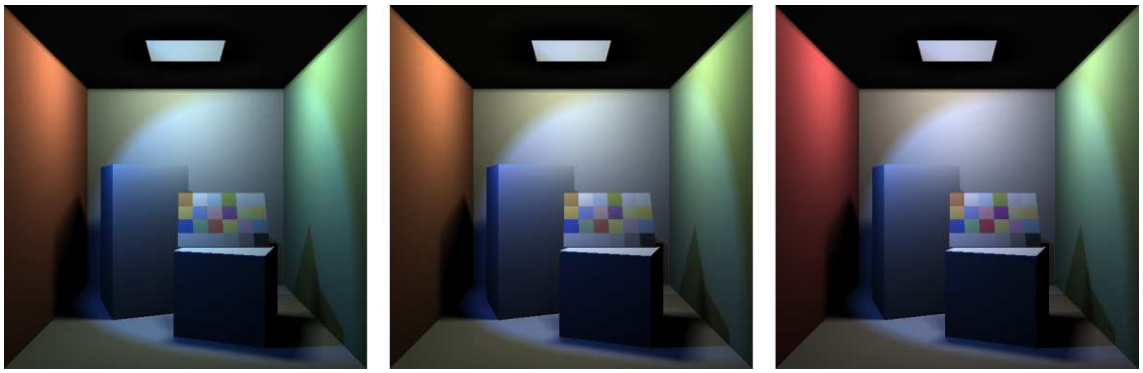

(b) Von Kries color correction

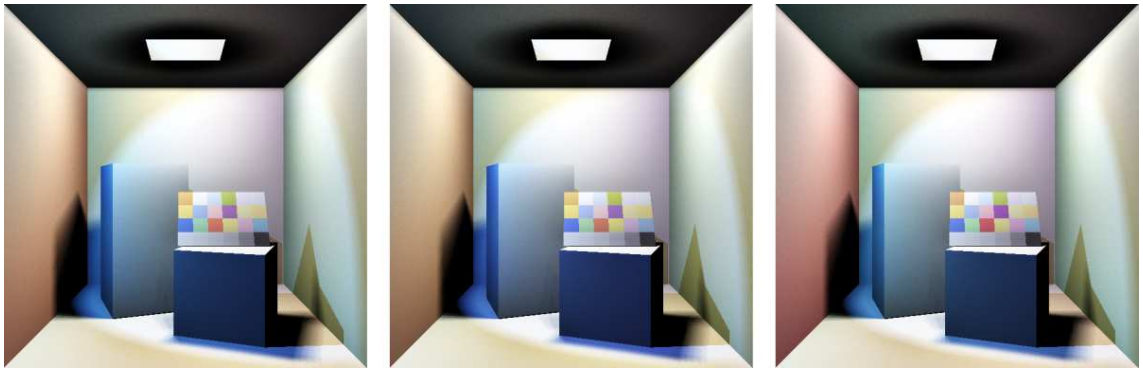

(c) Retinex color correction

Figure 5.10: *A/C illuminant. CIE RGB (left), Stiles and Burch (center) and Thornton (right) CMFs.*

Chapter 6

Conclusions

The purpose of this dissertation was to contribute in the color research field, with particular attention to the development of spatial color computation models based on the simulation of contextual color sensation mechanisms. After a preliminar overview (see chapter 2) of color research history (from the first proposals regarding color perception nature to the psycophysical analysis of color constany phenomenon) and of state of the art of computational models of color in context, we have presented the three main contributions of the dissertation.

Random Spray Retinex

In chapter 3 we have described the Random Spray Retinex (RSR) computational model.

The algorithm is based on a recent mathematical definition and analysis of the original Retinex algorithm, and it is characterized by the use of bidimensional *pixel sprays* instead of paths. This approach share the same intrinsic properties of every path-based Retinex implementation, but however is more suitable for the analysis of locality of color perception within the Retinex model, with better computational performance.

We have proposed an unsupervised method, validated through user panel tests, to tune RSR parameters for having correct results for all the possible input images; however, in same critical cases, they still strongly depend on the image content.

Future works on RSR will regard surely a more precise and automatic tuning of the parameters, probably considering some sort of preanalysis of the input images content, and the introduction in the computational model of lightness constancy mechanisms. Moreover, the application of RSR as tone mapping algorithm in under evaluation.

Finally, considering parallel nature of Retinex algorithms, we are modifying the original code for parallel computation on multicore architectures and GPU.

HDR Retinex

In chapter 4 we have discussed the lack and the need for color computation in the implementation of a correct tone mapping algorithm for High Dynamic Range images that tries to simulate perceptual response.

To this aim we have investigated how to change a path-based Retinex algorithm in order to tune its intrinsic color correction behavior for a correct mapping of HDR values into accepted dynamic range. We have proposed the HDR Retinex algorithm, based on the well-known and tested Brownian Retinex computational model, modified using paths roughly inspired by the eye movements and scene sampling, in order to avoid as possible halos and artifacts typical of spatial variant tone mapping operators.

We are considering as future works the introduction of adaptive weight mechanisms, based on the local contrast of the HDR input images, in the Retinex ratio-reset model, and, as for RSR algorithm, the implementation of HDR Retinex as a fragment shader for GPU computation.

Moreover, it would be very interesting the implementation of a eye-tracker ruled version of the algorithm for immersive Virtual Reality environments visualization.

Color Matching Functions interdifference and spatial color computation

Finally, in chapter 5, we have suggested as hypothesis that color perception mechanisms are able to compensate subjective differences in retinal color stimuli generation, due to the interpersonal variability in the spatial distribution of cones in human retina among different subjects.

We have proposed a computational experimental setup in order to evaluate the effect of spatial color computation applied on tristimulus values obtained using different Color Matching Functions (CMFs) to integrate spectral luminance distributions generated by a photometric raytracer.

The results of the presented experiments show a significant decrease of the difference induced in the tristimulus values by different CMFs when a contextual color correction is applied, confirming our initial hypothesis and therefore proving the extreme relevance of a correct spatial color computation in the imaging and computer graphics fields.

Acknowledgments

I thank *Ivar Farup, Alessandro Artusi* and *Majed Chambah* for having accepted to be referees of this dissertation, and for their comments and suggestions.

I thank my supervisors, *Daniele Marini* and *Alessandro Rizzi*, for their support and friendship in these years of work.

I thank *Lavinia* and *my parents*, for their love and support. To make them proud of me has been a great stimulus to continue during the bad days.

I thank all the friends that joined the "Eidolab" in Milan in these years for the great time spent, in particular *Davide Selmo, Marco Ronchetti, Massimiliano Piscozzi, Dario Villa, Alberto Viale*.

I thank all the people at Crema Department: *Carlo Gatta, Edoardo Provenzi, Max Fierro*, and at Politecnico of Milano: *Maurizio Rossi, Andrea Siniscalco, Cristina Fallica*, for their friendship and scientific collaborations.

I thank *Silvia Zuffi, Angelo Moretti, Claudio Oleari, Osvaldo da Pos* and *Tiziano Agostini* from the Italian Color Group for the interesting discussions on color perception during our last national conferences.

Bibliography

1. Albers, J.: *Interaction of colors*. Yale University Press, 1963.

2. Ashikhmin, M.: *A tone mapping algorithm for high contrast images*. In *Eurographics Workshop on Rendering*, 1–11. 2002.

3. Barnard, K. and Funt, B.: *Investigations into multi-scale retinex*. In *Colour Imaging: Vision and Technology*, 9–17. John Wiley and Sons, 1999.

4. Brainard, D. H. and Wandell, B. A.: *Analysis of the retinex theory of color vision*. J. Opt. Soc. Am. A, 3(10), 1651–1661, 1986.

5. Brainard, D. H. and Wandell, B. A.: *Asymmetric color matching: How color appearance depends on the illuminant*. J. Opt. Soc. Am., 9(9), 1433–1448, 1986.

6. Braun, J.: *Visual search among items of different salience: removal of visual attention mimics a lesion in extrastriate area V4*. Journal of Neuroscience, 14(2), 554–567, 1994.

7. Bresenham, J.: *Algorithm for computer control of a digital plotter*. IBM Systems Journal, 4(1), 1965.

8. Broadbent, A.: *A Critical Review of the Development of the CIE1931 RGB Color-Matching Functions*. Color Res. Appl., 29(4), 267–272, 2004.

9. Buchsbaum, G.: *A spatial processor model for object color perception*. J.Franklin inst., 310(1), 1–26, 1980.

10. Cater, K., Chalmers, A., and Ward, G.: *Detail to attention: Exploiting visual tasks for selective rendering.* In *Proceedings of the Eurographics Symposium on Rendering*, 270–280. 2003.

11. CELL architecture. URL research.scea.com/research/html/CellGDC05/.

12. Chalmers, A. and Cater, K.: *Realistic Rendering in Real-Time.* In *Euro-Par 2002 Parallel Processing*, 21–28. 2002.

13. Chevreul, M.: *The principles of harmony and contrast of colours, and their applications to the arts.* Henry G. Bohn, 1854.

14. Chiu, K., Herf, M., Shirley, P., Swamy, S., Wang, C., and Zimmerman, K.: *Spatially Non uniform Scaling Functions for High Contrast Images.* Proc. Graphics Interface '93, 245–253, 1993.

15. Choudhury, P. and Tumblin, J.: *The trilateral filter for high contrast images and meshes.* In *Proceedings of 14th Eurographics Workshop on Rendering*, 186–196. 2003.

16. *CIE Proceedings 1931.* Cambridge University Press, 19, 1932.

17. *CIE Proceedings 1963 (Vienna Session).* Committee Report E-1.4.1, B, 209–220, 1964.

18. Ciurea, F. and Funt, B.: *Tuning Retinex parameters.* Journal of Electronic Imaging, 13(1), 58–64, 2004.

19. Cooper, T. and Baqai, F. A.: *Analysis and extensions of the Frankle-McCann retinex algorithm.* Journal of Electronic Imaging, 13(1), 85–92, 2004.

20. Cooper, T. J.: *Modifications to retinex to relax reset nonlinearity and implement segmentation constraints.* In *Proc. of IS&T/SPIE's 14th Symposium on Electronic Imaging.* San Josè, California, 2002.

21. Cornell Box Website. URL www.graphics.cornell.edu/online/box/.

22. Courtney, S., Finkel, L., and Buchsbaum, G.: *Network simulations of retinal and cortical contributions to color constancy.* Vision Research, 35(3), 413–434, 1995.

23. Creutzfeld, O., Lange-Malecki, B., and Dreyer, E.: *Chromatic induction and brightness contrast: a relativistic color model.* J. Opt. Soc. Am. A, 7(9), 1644–1653, 1990.

24. Creutzfeld, O., Lange-Malecki, B., and Wortmann, K.: *Darkness induction, retinex and active mechanisms in vision.* Exp. Brain Res., 67, 270–283, 1987.

25. Debevec, P. and Malik, J.: *Recovering High Dynamic Range Radiance Maps from Photographs.* In *Proceedings of ACM Siggraph 1997*, 369–378. 1997.

26. Deubel, H.: *Separate adaptive mechanisms for the control of reactive and volitional saccadic eye movements.* Vision Research, 35, 3529–, 1995.

27. Drago, F., Myszkowski, K., Annen, T., and Chiba, N.: *Adaptive Logarithmic Mapping For Displaying High Contrast Scenes.* In *Proceedings of EUROGRAPHICS 2003*, 419–426. 2003.

28. Durand, F. and Dorsey, J.: *Fast bilateral filtering for the display of high-dynamic range images.* ACM Transactions on Computer Graphics (Proceedings of Siggraph 2002), 21(3), 257–267, 2002.

29. Engeldrum, P.: *Psychometric Scaling: A Toolkit for Imaging Systems Development.* ImcoTek Press, 2000.

30. Fairchild, M.: *A novel method for the determination of color matching functions.* Color Res. Appl., 14, 122–130, 1989.

31. Fairchild, M. D. and Johnson, G. M.: *Meet iCAM: An image color appearance model.* In *Proceedings of IS&T/SID 10th Color Imaging Conference*, 33–38. 2002.

32. Fairman, H. S., Brill, M. H., and Hemmendinger, H.: *How the CIE 1931 Color-Matching Functions Were Derived from Wright-Guild Data*. Color Res. Appl., 22(1), 11–23, 1997.

33. Fattal, R., Lischinski, D., and Werman, M.: *Gradient domain high dynamic range compression*. ACM Transactions on Computer Graphics (Proceedings of Siggraph 2002), 21(3), 249–256, 2002.

34. Ferraro, M., Boccignone, G., and Caelli, T.: *Entropy-based representation of image information*. Pattern Recognition Letters, 23(12), 1391–1398, 2002.

35. Ferwerda, J., Pattanaik, S., Shirley, P., and Greenberg, D.: *A Model of Visual Adaptation for Realistic Image Synthesis*. In *Proceedings of ACM Siggraph 1996*, 249–258. 1996.

36. Finlayson, G., Hordley, S., and Hubel, P.: *Color by Correlation: A Simple, Unifying Framework for Color Constancy*. IEEE Transactions on Pattern Analysis and Machine Intelligence, 23(11), 1209–1221, 2001.

37. Frankle, J. and McCann, J.: *Method and Apparatus for Lightness Imaging*. US Patent 4.384.336, 1983.

38. Funt, B., Ciurea, F., and McCann, J.: *Retinex in MATLAB^{TM}*. Journal of Electronic Imaging, 13(1), 48–57, 2004.

39. Gadia, D., Marini, D., and Rizzi, A.: *Tuning Retinex for HDR Images Visualization*. In *Proceedings of CGIV04, IS&T Second European Conference on Color in Graphics, Imaging and Vision*, 326–331. Aachen, Germany, 2004.

40. Gatta, C.: *Human Visual System Color Perception Models and Applications to Computer Graphics*, 2005. PhD Thesis - Università degli Studi di Milano.

41. Gatta, C., Rizzi, A., and Marini, D.: *Local linear LUT method for spatial colour-correction algorithm speed-up*. IEE Proceedings Vision, Image & Signal Processing., 153(3), 357–363, 2006.

42. Gilchrist, A., Kossyfidis, C., Bonato, F., Agostini, T., Cataliotti, J., Li, X., Spehar, B., Annan, V., and Economou, E.: *An anchoring theory of lightness perception.* Psychological Review, 106(4), 795–834, 1999.

43. Goethe, J.: *Theory of Colours.* MIT Press, 1982.

44. Goodnight, N., Wang, R., Woolley, C., and Humphreys, G.: *Interactive Time-Dependent Tone Mapping Using Programmable Graphics Hardware.* In *Rendering Techniques*, 26–37. 2003.

45. Goral, C., Torrance, K., Greenberg, D., and Battaile, B.: *Modeling the interaction of light between diffuse surfaces.* ACM Transactions on Computer Graphics (Proc. Siggraph '84), 18(3), 213–222, 1984.

46. GPGPU Website. URL www.gpgpu.org.

47. Hering, E.: *Outlines of a Theory of the Light Sense.* Harvard University Press, 1964.

48. Hofer, H., Carroll, J., Neitz, J., Neitz, M., and Williams, D. R.: *Organization of the Human Trichromatic Cone Mosaic.* Journal of Neuroscience, 25(42), 9669–9679, 2005.

49. Hu, X. and Houser, K. W.: *Large-Field Color Matching Functions.* Color Res. Appl., 31(1), 18–29, 2006.

50. Hurvich, L. and Jameson, D.: *Theory of brightness and color contrast in human vision.* Vision Research, 4, 135–154, 1990.

51. Ilg, U.: *Slow eye movements.* Progress in Neurobiology, 53, 293–, 1997.

52. Itti, L. and Niebur, E.: *A model of saliency-based visual attention for rapid scene analysis.* Pattern Analysis and Machine Intelligence, 20, 1254–1259, 1998.

53. Jobson, D., Rahman, Z., and Woodell, G.: *Properties and Performance of a Center/Surround Retinex.* IEEE Trans. Image Processing, 6(3), 451–462, 1997.

54. Jobson, D. J., Rahman, Z., and Woodell, G. A.: *A multiscale Retinex for bridging the gap between color images and the human observation of scenes.* IEEE Transactions on Image Processing, 6(7), 965–976, 1997.

55. Johnson, G. M. and Fairchild, M. D.: *Rendering HDR images.* In *Proceedings of IS&T/SID 11th Color Imaging Conference*, 36–41. 2003.

56. Judd, D.: *Report of U.S. Secretariat Committee on Colorimetry and Artificial Daylight.* In *Proceedings of the Twelfth Session of the CIE*, 11–. Stockholm, 1951.

57. Kang, S. B., Uyttendaele, M., Winder, S., and Szeliski, R.: *High dynamic range video.* ACM Transactions on Computer Graphics (Proceedings of Siggraph 2003), 22(3), 319–325, 2003.

58. Koch, C. and Ullman, S.: *Shifts in selective visual attention: towards the underlying neural circuitry.* Human Neurobiology, 4, 219–227, 1985.

59. Kowler, E.: *The role of attention in the programming of saccades.* Vision Research, 35, 1897–, 1995.

60. Krawczyk, G., Myszkowski, K., and Seidel, H.: *Lightness Perception in Tone Reproduction for High Dynamic Range Images.* In *Proceedings of EuroGraphics 2005*. 2005.

61. Krawczyk, G., Myszkowski, K., and Seidel, H.: *Perceptual Effects in Real-Time Tone Mapping.* In *Proceedings of 21st ACM Spring Conference on Computer Graphics*, 195–202. 2005.

62. Krawczyk, G., Myszkowski, K., and Seidel, H.: *Computational Model of Lightness Perception in High Dynamic Range Imaging.* In *Human Vision and Electronic Imaging XI, Proc. of IS&T/SPIE's 18th Symposium on Electronic Imaging.* San Josè, California, 2006.

63. Land, E.: *The Retinex Theory of Color Vision.* Scientific American, 237(6), 1977.

64. Land, E.: *Recent advances in retinex theory and some implications for cortical computations: Color vision and the natural image.* Proc. Nat. Acad. Sci., 80, 5163–5169, 1983.

65. Land, E.: *An alternative technique for the computation of the designat in the retinex theory of color vision.* In *Proc. Natl. Acad. Sci.*, 3078–3080. 1986.

66. Land, E. and MCCann, J.: *Lightness and retinex theory.* J.Opt.Soc.Am, 63(1), 1–11, 1971.

67. Land, M., Mennie, N., and Rusted, J.: *The roles of vision and eye movements in the control of activities of daily living.* Perception, 28, 1311–1328, 1999.

68. Marini, D. and Rizzi, A.: *A computational approach to color illusions.* Image Analysis and Processing, 62–69, 1997.

69. Marini, D. and Rizzi, A.: *A computational approach to color adaptation effects.* Image and Vision Computing, 18, 1005–1014, 2000.

70. Marini, D., Rizzi, A., and DeCarli, L.: *Multiresolution retinex: comparison of algorithms.* In *Proc. CGIP'2000, First International Conference on Color in Graphics and Image Processing.* Saint-Etienne, FRANCE, 2000.

71. Marmitt, G. and Duchowski, A.: *Modeling visual attention in VR: Measuring the accuracy of predicted scanpaths.* In *Proceedings of EuroGraphics 2002 Short Papers*, 217–226. 2002.

72. Maxwell, J. C.: *On the Theory of Compound Colours, and the Relations of the Colours of the Spectrum.* Color Res. Appl., 18(4), 270–287, 1993.

73. McCann, J.: *The role of simple nonlinear operations in modelling human lightness and color sensation.* In *SPIE Proceedings 1077 - Human Vision, Visual Processing and Digital Display.* 1989.

74. McCann, J.: *Lesson Learned from Mondrians Applied to Real Images and Color Gamuts*. In *Proc. IS&T/SID 7th Color Imaging Conference*, 1–8. Scottsdale, Arizona (USA), 1999.

75. McNamara, A.: *Visual perception in realistic image synthesis*. In *STAR - State of The Art Report - Proc. of Eurographics 2000*. 2000.

76. Meylan, L. and Susstrunk, S. E.: *High Dynamic Range Image Rendering Using a Retinex-Based Adaptive Filter*. IEEE Transactions on Image Processing, 15(9), 2820–2830, 2006.

77. Monge, G.: *Mémoire sur quelques phénomenès de la vision*. Annales de Chimie, 3, 131–147, 1789.

78. Moore, A., Allman, J., and Goodman, R.: *A real-time neural system for color constancy*. IEEE Transaction on Neural Networks, 2(2), 237–246, 1991.

79. Navalpakkam, V. and Itti, L.: *A goal oriented attention guidance model*. In *Proceedings of the Second International Workshop on Biologically Motivated Computer Vision*, 453–461. 2002.

80. Navalpakkam, V. and Itti, L.: *Modeling the influence of task on attention*. Vision Research, 45(2), 205–231, 2005.

81. Newton, I.: *Opticks: Or, A Treatise of the Reflexions, Refractions, Inflexions and Colours of Light*. Smith and Waltford, 1704.

82. North, A. and Fairchild, M.: *Measuring color-matching functions. Part I*. Color Res. Appl., 18, 155–162, 1993.

83. North, A. and Fairchild, M.: *Measuring color-matching functions. Part II*. Color Res. Appl., 18, 163–170, 1993.

84. OpenMP Website. URL www.openmp.org/drupal/.

85. O'Sullivan, C., Howlett, S., Morvan, Y., McDonnel, R., and O'Conor, K.: *Perceptually adaptive graphics.* In *STAR - State of The Art Report - Proceedings of Eurographics 2004*, 141–164. 2004.

86. Oulton, D.: *The Properties of Multiple CMF Determinations Using Alternative Primary Sets Part I: Evidence and Modeling.* Color Res. Appl., 29(4), 273–284, 2004.

87. Oulton, D.: *The Properties of Multiple CMF Determinations Using Alternative Primary Sets Part II: A Data Unification Methodology.* Color Res. Appl., 29(6), 438–450, 2004.

88. Pattanaik, N., Ferwerda, J., Fairchild, M., and Greenberg, D.: *A multiscale model of adaptation and spatial vision for realistic image display.* In *Proceedings of ACM Siggraph 1998*, 287–298. 1998.

89. Provenzi, E., DeCarli, L., Rizzi, A., and Marini, D.: *Mathematical definition and analysis of the Retinex algorithm.* J. Opt. Soc. Am. A, 22, 2613–2621, 2005.

90. Provenzi, E., Fierro, M., Rizzi, A., DeCarli, L., Gadia, D., and Marini, D.: *Random Spray Retinex: a new Retinex implementation to investigate the local properties of the model.* IEEE Transactions on Image Processing, 16(1), 162–171, 2007.

91. Reinhard, E. and Devlin, K.: *Dynamic range reduction inspired by photoreceptor physiology.* IEEE Transaction on Visualization and Computer Graphics, 11(1), 13–24, 2005.

92. Reinhard, E., Stark, M., Shirley, P., and Ferwerda, J.: *Photographic tone reproduction for digital images.* ACM Transactions on Computer Graphics (Proceedings of Siggraph 2002), 21(3), 267–276, 2002.

93. Reinhard, E., Ward, G., Pattanaik, S., and Debevec, P.: *High dynamic range imaging.* Elsevier / Morgan Kaufmann, 2005.

94. Rensink, R.: *Visual attention.* In *Encyclopedia of Cognitive Science.* Nature Publishing Group, London, 2003.

95. Rising, H. K.: *Analysis and generalization of retinex by recasting the algorithm in wavelets.* In *Human Vision and Electronic Imaging VII, Proc. of IS&T/SPIE's 14th Symposium on Electronic Imaging*, 419–427. San Josè, California, 2002.

96. Rizzi, A., Gadia, D., and Marini, D.: *Analysis of tristimulus interdifference and contextual color correction.* Journal of Electronic Imaging - Special Section - Color Imaging: Processing, Hard Copy, and Applications, 15(4), 2006.

97. Rizzi, A., Gatta, C., and Marini, D.: *A new algorithm for unsupervised global and local color correction.* Pattern Recognition Letters., 124, 1663–1677, 2003.

98. Rizzi, A., Gatta, C., and Marini, D.: *Yaccd: Yet another color constancy database.* In *Color Imaging VIII, Proc. of IS&T/SPIE's 15th Symposium on Electronic Imaging*, 24–35. San Josè, California, 2003.

99. Rizzi, A., Gatta, C., Piacentini, B., Fierro, M., and Marini, D.: *Human-visual-system-inspired tone mapping algorithm for HDR images.* In *Human Vision and Electronic Imaging IX, Proc. of IS&T/SPIE's 16th Symposium on Electronic Imaging*, 57–68. San Josè, California, 2004.

100. Ross, W. and Mingolla, E.: *Recent progress in modeling neural mechanisms of form and color vision.* Image and Vision Computing, 16, 447–472, 1998.

101. Rossi, M., Marini, D., and Rizzi, A.: *Methods and application for photorealistic rendering and lighting of ancient buildings.* Journal of Cultural Heritage, 5(3), 291–300, 2004.

102. Saupe, D.: *Algorithms for random fractals.* In *The Science of Fractal Images.* Springer Verlag, New York, 1988.

103. Schlick, C.: *Quantization Techniques for Visualization of High Dynamic Range Pictures*. Photorealistic Rendering Techniques, 7–20, 1995.

104. Sobol, R.: *Improving the Retinex algorithm for rendering wide dynamic range photographs*. Journal of Electronic Imaging, 13(1), 65–74, 2004.

105. Speranskaya, N. I.: *Determination of spectrum color coordinates for twenty-seven normal observers*. Optics and Spectroscopy, 7, 424–428, 1959.

106. Spheron Website. URL www.spheron.com.

107. Spitzer, H. and Semo, S.: *Color constancy: a biological model and its application for still and video images*. Pattern Recognition Letters, 35(8), 1645–1659, 2002.

108. Stiles, W. S. and Burch, J. M.: *NPL colour-matching investigation: Final report*. Optica Acta, 6, 1–26, 1959.

109. Stockman, A., MacLeod, D., and Johnson, N.: *Spectral sensitivities of the human cones*. J. Opt. Soc. Am. A, 10(12), 2491–2521, 1993.

110. Sundstedt, V. and Chalmers, A.: *Evaluation of Perceptually-Based Selective Rendering Techniques using Eye-Movements Analysis*. In *Proceedings of ACM SCCG 2006 - Spring Conference on Computer Graphics*. 2006.

111. Sundstedt, V., DeBattista, K., Longhurst, P., Chalmers, A., and Troscianko, T.: *Visual attention for efficient high-fidelity graphics*. In *Proceedings of Spring Conference on Computer Graphics*, 162–168. 2005.

112. Thornton, W. A.: *Toward a more accurate and extensible colorimetry: Part I*. Color Res. Appl., 17, 79–122, 1992.

113. Thornton, W. A.: *Toward a more accurate and extensible colorimetry: Part II*. Color Res. Appl., 17, 240–262, 1992.

114. Thornton, W. A.: *Toward a more accurate and extensible colorimetry: Part III*. Color Res. Appl., 17, 162–186, 1992.

115. Thornton, W. A.: *Toward a more accurate and extensible colorimetry: Part IV.* Color Res. Appl., 22(3), 189–198, 1997.

116. Thornton, W. A.: *Toward a more accurate and extensible colorimetry: Part VI.* Color Res. Appl., 23(4), 226–233, 1998.

117. Thornton, W. A.: *Spectral Sensitivities of the Normal Human Visual System, Color-Matching Functions and Their Principles, and How and Why the Two Sets Should Coincide.* Color Res. Appl., 24(2), 139–156, 1999.

118. Thornton, W. A. and Fairman, H. S.: *Toward a more accurate and extensible colorimetry: Part V.* Color Res. Appl., 23(2), 92–103, 1998.

119. Trezona, P.: *Derivation of the 1964 CIE 10° XYZ Colour-Matching Functions and Their Applicability in Photometry.* Color Res. Appl., 26(1), 67–75, 2001.

120. Trezona, P. and Parkins, R.: *Derivation of the 1964 Colorimetric Standards.* Color Res. Appl., 23(4), 221–225, 1998.

121. Tumblin, J., Hodgins, J., and Guenter, B.: *Two methods for display of high contrast images.* ACM Transactions On Graphics, 18(1), 56–94, 1999.

122. Tumblin, J. and Rushmeier, H.: *Tone Reproduction for Realistic Images.* IEEE Computer Graphics and Applications, 13(6), 42–48, 1993.

123. Tumblin, J. and Turk, G.: *LCIS:A boundary hierarchy for detail-preserving contrast reduction.* In *Proc. of ACM Siggraph 1999*, 83–90. 1999.

124. von Helmholtz, H.: *Wissenschaftliche Abhandlungen von Hermann von Helmholtz.* J.A. Barth, 1892-1895.

125. von Kries, J.: *Sources of Color Science.* In *Chromatic adaptation*, 109–119. MIT Press, Cambridge, MA, 1970.

126. Vos, J.: *Colorimetric and photometric properties of a 2° fundamental observer.* Color Res. Appl., 3, 125–128, 1978.

127. Wandell, B.: *Foundations of Vision.* Sinauer Associates Inc. Publishers, Sunderland, Massachusetts, 1995.

128. Ward, G.: *A Contrast-Based Scale factor for Luminance Display.* Graphics Gems IV, 415–421, 1994.

129. Ward, G., Rushmeier, H., and Piatko, C.: *A visibility matching tone reproduction operator for high dynamic range scenes.* IEEE Transactions on Visualization and Computer Graphics, 3(4), 291–306, 1997.

130. Wassef, E.: *Linearity of the relationship between the tristimulus values of corresponding colours seen under different conditions of chromatic adaptation.* Optica Acta, 6, 378–393, 1959.

131. Wyszecky, G. and Stiles, W. S.: *Color Science: Concepts and Methods, Quantitative Data and Formulas.* J. Wiley & Sons, New York, 1982.

132. Yarbus, A.: *Eye movements and vision.* Plenum Press, New York, 1967.

133. Young, T.: *On the Theory of Light and Colours.* Philosophical Transactions Royal Society, 92, 12–48, 1802.

134. Zaidi, Q.: *Color and brightness induction: From Mach bands to 3-D configurations.* In *Color Vision: From Genes to Perception.* Cambridge University Press, New York, 1999.

135. Zangemeister, W.: *Evidence for a global scanpath strategy in viewing abstract compared with realistic images.* Neuropsychologia, 33, 1009–, 1995.

136. Zeki, S.: *A Vision of the Brain.* Blackwell Scientific Pub., Oxford, 1993.